Vélez Rasero, Paris; Canalias, Xavier; Muñoz Enano, Jonathan; [et al.]. «Effects of losses on the sensitivity of reflective-mode phase-variation liquid sensors». IEEE transactions on microwave theory and techniques, Vol. 72, no. 2 (February 2024), p. 903-908. DOI 10.1109/TMTT.2023.3308586

# Effects of Losses on the Sensitivity of Reflective-Mode Phase-Variation Liquid Sensors

Paris Vélez, *Senior Member, IEEE*, Xavier Canalias, Jonathan Muñoz-Enano, *Member, IEEE*, Pau Casacuberta, *Graduate Student Member, IEEE*, Lijuan Su, *Member IEEE*, and Ferran Martín, *Fellow, IEEE*

***Abstract*— This paper is focused on the analysis of the effects of losses on the sensitivity of reflective-mode phase-variation liquid sensors implemented by means of an open-ended (either quarter-wavelength or half-wavelength) transmission line distributed resonator (the sensing element) cascaded to a set of high/low impedance inverters (implemented by means of quarter-wavelength line sections). The device operates at a single frequency and the working principle is the variation of the phase of the reflection coefficient (the output variable) caused by changes in the dielectric properties of the material under test (MUT), a liquid in the present study. Since liquids are lossy samples, it is expected that the sensitivity of the sensor is influenced by losses, an aspect demonstrated in this paper. It is shown that two operation regimes can be distinguished: (i) the low-loss regime, where the sensitivity is influenced by MUT losses, but the behavior is similar to the one of the lossless case; and (ii) the high-loss regime, where losses not only play a key role on the sensitivity, but also modify the dependence of the output variable with the dielectric constant of the liquid under consideration, as compared to the lossless case. Nevertheless, contrarily to general belief, with an adequate sensor design, losses might be beneficial in order to boost up the sensitivity in the limit of small perturbations (this is the main contribution of this paper). Validation is carried out by considering different types of oil samples, and various sensing devices operating either in the low-loss or in the high-loss regime.**

***Index Terms*— dielectric losses, microstrip technology, microwave sensors, permittivity sensors, phase-variation sensors.**

## I. INTRODUCTION

PLANAR microwave sensors have been the subject of an intensive research activity in recent years [1], [2]. The main reasons are their low cost and profile, their robustness against operation in harsh environments (e.g., with pollution and dirtiness), their compatibility with other technologies (e.g., microfluidics, substrate integrated waveguides, textiles, micromachining, 3D-printing, etc.) and many types of substrates (rigid, flexible, polymeric, paper, etc.), and their inherent wireless connectivity, among others. Since microwaves are very sensitive to the dielectric properties of the materials to which they interact, microwave sensors have been mainly devoted to the measurement of material permittivity and other variables related to it, including physical variables (e.g., temperature [3], [4], humidity [5], [6], etc.), chemical variables (e.g., gas concentration [7], [8], material composition [9]-[12], etc.), or biological variables (e.g., glucose concentration [13], [14], electrolyte concentration [15], [16], bacterial growth [17], [18], monitoring the denaturation of proteins [19], etc.). Nevertheless, other applications of planar microwave sensors, such as the measurement of spatial variables (displacements and velocities) [20]-[26], or even, the monitoring of vital signs (e.g., [27], [28]), have been reported.

This diversity of applications of planar microwave sensors has been achieved by considering different working principles, with their pros and cons, mainly including frequency variation [9], [29]-[38], frequency splitting [39]-[43], coupling modulation [20], [23], [44]-[53], and phase variation [24], [54]-[73]. Though most planar microwave sensors are based on resonant elements and exploit the resonance frequency variation experienced by the sensing (resonant) element due to changes in its immediate surrounding, such sensors require wideband signals for sensing (the sweeping interrogation signal must cover the output dynamic range). This might represent a limitation in operational environment, due to the increase in the cost of the associated electronics (wideband voltage-controlled oscillators –VCOs–, or arrays of VCOs, are needed). Such limitative aspect applies also to frequency-splitting sensors. Thus, single-frequency sensors, such as coupling-modulation sensors and phase-variation sensors are of high interest. Indeed, phase-variation sensors combine the advantages of single-frequency sensors with the robustness against electromagnetic interference (EMI) and noise inherent to phase measurements (and to frequency measurements). By contrast, in coupling modulation sensors, the output variable is typically the magnitude of the transmission or reflection coefficient of the sensing device (or a voltage, provided an amplitude detector is included), less tolerant to the effects of EMI and noise.

The previous advantageous aspects of phase-variation sensors, and the highly achievable sensitivity, especially in one-port sensors operating in reflection mode, have motivated a significant research activity focused on the optimization of phase-variation sensors. Unprecedented sensitivities with the

This work was supported by MCIN/AEI 10.13039/501100011033, Spain, through projects PID2019-103904RB-I00, PID2022-139181OB-I00 (ERDF European Union) and PDC2021-121085-I00 (European Union Next Generation EU/PRTR), by Agència Catalana d'Ajuts Universitaris i de Recerca (AGAUR), Catalonia Government, through project 2021-SGR00192, and by Institució Catalana de Recerca i Estudis Avançats (ICREA). P. Casacuberta acknowledges the Ministerio de Universidades, Spain, for the FPU grant (Ayudas para la formación de profesorado universitario), ref. FPU20/05700. L. Su acknowledges the Juan de la Cierva Program for the support through the project IJC2019-040786-I

The authors are with CIMITEC, Departament d'Enginyeria Electrònica, Universitat Autònoma de Barcelona, 08193 Bellaterra, Spain.

Color versions of one or more of the figures in this article are available online at http://ieeexplore.ieee.org.

dielectric constant of the material under test (MUT), the canonical input variable, have been achieved by considering reflective-mode phase-variation sensors based on two different approaches. One of such approaches, first presented in [63], uses a sensing resonator (either distributed [63]-[65], or semi-lumped [66], [67]) as termination of a set of cascaded high/low impedance inverters (implemented by means of quarter-wavelength transmission lines). In the other approach, a pair of weakly coupled resonators (either distributed [69] or semi-lumped [70]) is considered for sensing. In both cases, maximum sensitivities of hundreds of degrees per unit of dielectric constant have been reported [63], [69]. In the sensors proposed in [63]-[70], the considered MUTs were low-loss solid samples. It was demonstrated in [63] that the effects of MUT losses on the sensor response and sensitivity are not significant provided losses are small (and hence losses were neglected in those works). However, for certain materials, such as liquids (in general, exhibiting high loss factors), this low-loss assumption might not be valid.

In this paper, the effects of MUT losses on the sensitivity of one-port reflective-mode phase-variation sensors based on a cascade of high/low impedance inverters terminated with a distributed resonator (either an open-ended quarter- or a half-wavelength sensing line) are studied analytically. The main conclusions of such analysis are validated through full-wave electromagnetic simulation and experimentally, by considering various oil samples. Note that oils are liquids exhibiting a non-negligible loss tangent and are therefore very appropriate for the present study. The main goal of the paper is to provide a guide on how to design a sensor taking advantage of the losses of the intended material to be measured (oils in this paper) for sensitivity optimization.

The paper is organized as follows. The sensor under study and the sensitivity analysis by including the effects of losses in the MUT are the subject of Section II. Section III presents the specific designed and fabricated sensors, based on a fluidic channel made of methacrylate and validates the sensitivity analysis. A discussion, mainly devoted to compare the sensors of this work with other phase variation sensors is carried out in Section IV. Finally, Section V concludes the work.

## II. The Proposed Reflective-Mode Phase-Variation Liquid Sensor and Sensitivity Analysis by Including MUT Losses

Figure 1 depicts a perspective view (sketch), a typical layout (microwave module), and the circuit schematic of the proposed liquid sensor. The microwave module (implemented in microstrip technology) consists of a one-port structure including the access line (matched to the reference impedance of the port, $Z_0$ = 50 Ω in this work), the cascade of $N$ impedance inverters (implemented by means of quarter-wavelength transmission line sections) with alternating high and low characteristic impedance, denoted as $Z_i$ (with $i$ = 1… $N$), and the sensing line (an open-ended quarter- or half-wavelength distributed resonator). The impedance $Z_s$ and electrical length $\phi_s$ of the sensing line both depend on the dielectric properties of the material under study. Note that in the specific sketch and layout of Fig. 1, a single inverter is considered (i.e., $N$ = 1), but the number of inverters can be arbitrary [see Fig. 1(c)]. The sensing region is indicated by the dashed rectangle in the layout. Thus, the liquid (fluidic) channel should be placed on top of it, so that the liquid under test (LUT from now on) is in contact with the sensitive element.

The working principle of the sensor is the variation in the phase of the reflection coefficient caused by changes in the dielectric constant of the LUT placed in the fluidic channel. It was demonstrated in [63] that in the limit of small perturbations of the dielectric constant of the LUT ($\varepsilon_{LUT}$) in the vicinity of the reference REF dielectric constant ($\varepsilon_{REF}$), the sensitivity is optimized by considering either a high-impedance open-ended quarter-wavelength transmission line sensing resonator [the case of Fig. 1(a) and (b)] or a low-impedance open-ended half-wavelength transmission line sensing resonator (in both cases corresponding to a high $Q$-resonator). The reason is that, under these conditions, the phase slope at resonance ($f_0$, the operating frequency) is high. This generates a significant excursion of the phase of the reflection coefficient at $f_0$ (the output variable) when the dielectric constant of the LUT varies (note that a lateral shift in the phase response caused by a change in $\varepsilon_{LUT}$ generates an important phase variation at a fixed frequency, in particular, at $f_0$, if the phase slope at that frequency is high). Let us clarify that the nominal electrical length of the sensing line, $\phi_s$ (either 90º or 180º), corresponds to the situation where such line is coated with the REF liquid.

It was also shown in [63] that the sensitivity in the limit of small perturbations can be further optimized by cascading a set of impedance inverters, with alternating high and low impedance, between the sensing line resonator and the access line. A requirement of such inverters (in practice implemented by means of quarter-wavelength transmission line sections, so that $\phi_i$ = 90º) is that the impedance of the inverter adjacent to the sensing line, $Z_1$, should be low if the sensing line is a high-impedance open-ended quarter-wavelength resonator, and it should be high when the sensing line is a low-impedance open-ended half-wavelength resonator. The higher the impedance contrast of the quarter-wavelength line sections (inverters), including the sensing line, the optimum the sensitivity in the limit of small perturbations [63].

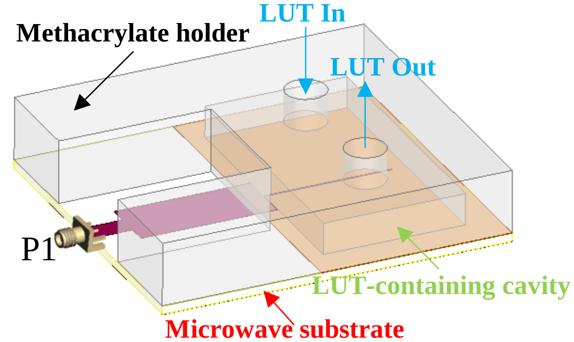

(a)

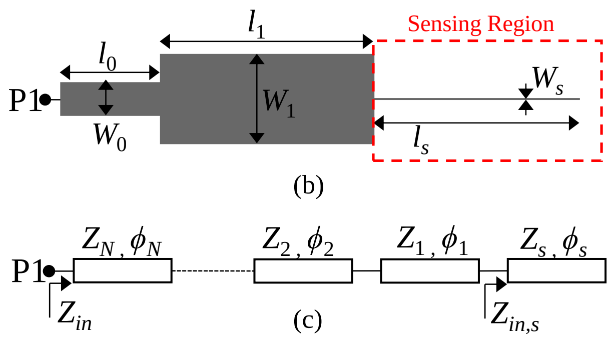


**Fig. 1.** Proposed liquid sensor. (a) Sketch of the perspective view; (b) typical layout; (c) circuit schematic by considering $N$ impedance inverters, excluding the access line. Relevant dimensions are indicated in (b). In (a) and (b) a single inverter ($N$ = 1) is considered. Length $l_0$ and width $W_0$ correspond to the access line, whereas for the inverter stages such dimensions are designated as $l_i$ and $W_i$ (the subindex $i$ specifying the inverter).

Let us next focus on the sensitivity analysis by including the effects of losses in the MUT (LUT for the specific case under study, provided we deal with liquid samples). The sensitivity is defined as the derivative of the output variable with regard to the input variable, i.e.,

$$S = \frac{d\phi_\rho}{d\varepsilon_{\text{LUT}}} \quad (1)$$

where $\phi_\rho$ is the phase of the reflection coefficient at $f_0$. As pointed out in [63], such derivative can be expressed as

$$S = \frac{d\phi_\rho}{d\phi_s}\cdot\frac{d\phi_s}{d\varepsilon_{\text{LUT}}} + \frac{d\phi_\rho}{dZ_s}\cdot\frac{dZ_s}{d\varepsilon_{\text{LUT}}} \quad (2)$$

since a variation in $\varepsilon_{\text{LUT}}$ is expected to perturb $\phi_\rho$ through a modification of both the electrical length, $\phi_s$, and characteristic impedance, $Z_s$, of the sensing line. However, $d\phi_\rho/dZ_s = 0$ when the electrical length of the sensing line is a multiple of $\pi/2$ (the cases under consideration) [63]. Consequently, only the first term of the right-hand side member of (2) must be retained. To calculate the sensitivity, the first step is to express the input impedance of the sensor as a function of the different electrical parameters of the constitutive lines. By excluding the access line, which only generates a constant phase shift in the reflection coefficient (and, thus, its effects can be neglected), the input impedance can be expressed as

$$Z_{in} = \{Z_{in,s}\}^{(-1)^N}\cdot\prod_{i=1}^{N} Z_i^{2(-1)^{i+N}} \quad (3)$$

where $Z_{in,s}$ is the impedance seen from the input port of the sensing line, see Fig. 1(c), and $Z_i$ (with $i$ = 1, 2, 3…$N$) are the characteristic impedances of the cascaded high/low quarter-wavelength (at $f_0$) line sections (impedance inverters), as mentioned. By considering losses in the sensing line (mainly caused by the presence of the LUT on top of it) the impedance $Z_{in,s}$ can be expressed as shown in [74]

$$Z_{in,s} = Z_s \coth \gamma l_s \quad (4)$$

where $\gamma = \alpha + j\beta$ is the complex propagation constant ($\alpha$ and $\beta$ being the attenuation constant and the phase constant, respectively, of the sensing line), and $l_s$ is the physical length of such line (i.e., $\phi_s = \beta l_s$). After some simple algebra, expression (4) can be written as

$$Z_{in,s} = Z_s\frac{\sinh 2\alpha l_s - j\sin 2\phi_s}{\cosh 2\alpha l_s - \cos 2\phi_s} \quad (5)$$

The reflection coefficient seen from the input port of the sensor (excluding the access line) is:

$$\rho = \frac{Z_{in} - Z_0}{Z_{in} + Z_0} \quad (6)$$

Let us first calculate the phase of the reflection coefficient and the sensitivity by considering that the sensing line is directly connected to the input port, i.e., without impedance inverters ($N$ = 0), and then we will generalize to the case of a sensor with an arbitrary number $N$ of impedance inverters. With $N$ = 0, $Z_{in} = Z_{in,s}$, and the reflection coefficient is

$$\rho = \frac{Z_s\dfrac{\sinh 2\alpha l_s - j\sin 2\phi_s}{\cosh 2\alpha l_s - \cos 2\phi_s} - Z_0}{Z_s\dfrac{\sinh 2\alpha l_s - j\sin 2\phi_s}{\cosh 2\alpha l_s - \cos 2\phi_s} + Z_0} \quad (7)$$

which in turn can be expressed as

$$\rho = \frac{Z_s\sinh 2\alpha l_s - Z_0(\cosh 2\alpha l_s - \cos 2\phi_s) - jZ_s\sin 2\phi_s}{Z_s\sinh 2\alpha l_s + Z_0(\cosh 2\alpha l_s - \cos 2\phi_s) - jZ_s\sin 2\phi_s} \quad (8)$$

where the real and the imaginary parts in the numerator and the denominator are separated, in order to calculate the phase of the reflection coefficient. Note that, though losses are taken into account, it is considered that the characteristic impedance of the sensing line, $Z_s$, is a real number, a reasonable (and accepted) approximation. Let us also indicate that losses, accounted for by means of $\alpha$, also include ohmic losses (generally small in transmission lines) and radiation losses.

The phase of the reflection coefficient is:

$$\phi_\rho = \phi_N - \phi_D \quad (9)$$

where $\phi_N$ and $\phi_D$ are the phase of the numerator and the phase of the denominator, respectively, in (8), given by

$$\phi_N = \arctan\left(\frac{Z_s\sin 2\phi_s}{Z_0(\cosh 2\alpha l_s - \cos 2\phi_s) - Z_s\sinh 2\alpha l_s}\right) \quad (10a)$$

$$\phi_D = -\arctan\left(\frac{Z_s\sin 2\phi_s}{Z_0(\cosh 2\alpha l_s - \cos 2\phi_s) + Z_s\sinh 2\alpha l_s}\right) \quad (10b)$$

Let us next calculate the derivative $d\phi_\rho/d\phi_s$, i.e., the first term in the sensitivity, as given by (2). Such derivative can be expressed as

$$\begin{aligned}\frac{d\phi_\rho}{d\phi_s} &= \frac{1}{1+\left(\frac{N}{D_1}\right)^2}\frac{2Z_sD_1\cos 2\phi_s - 2Z_0N\sin 2\phi_s}{D_1^2} + \\ &+ \frac{1}{1+\left(\frac{N}{D_2}\right)^2}\frac{2Z_sD_2\cos 2\phi_s - 2Z_0N\sin 2\phi_s}{D_2^2}\end{aligned} \quad (11)$$

where the following terms have been defined in order to simplify the formulas

$$N = Z_s \sin 2\phi_s \tag{12a}$$

$$D_1 = Z_0 (\cosh 2\alpha l_s - \cos 2\phi_s) - Z_s \sinh 2\alpha l_s \tag{12b}$$

$$D_2 = Z_0 (\cosh 2\alpha l_s - \cos 2\phi_s) + Z_s \sinh 2\alpha l_s \tag{12c}$$

Since the interest is the calculation of the sensitivity in the limit of small perturbations in the vicinity of the dielectric constant of the REF liquid, and the sensor should be designed in order to exhibit a sensing line length of either a quarter-wavelength (or an odd multiple), or a half-wavelength (or any multiple), we should evaluate (11) for phases satisfying either $\phi_s = (2n + 1)\cdot\pi/2$ or $\phi_s = n\cdot\pi$. The following results are obtained:

$$\left.\frac{d\phi_\rho}{d\phi_s}\right|_{\phi_s=(2n+1)\cdot\pi/2} = -\frac{2Z_sZ_0}{Z_0^2\cosh^2\alpha l_s - Z_s^2\sinh^2\alpha l_s} \tag{13a}$$

$$\left.\frac{d\phi_\rho}{d\phi_s}\right|_{\phi_s=n\cdot\pi} = -\frac{2Z_sZ_0}{Z_s^2\cosh^2\alpha l_s - Z_0^2\sinh^2\alpha l_s} \tag{13b}$$

To calculate the sensitivity (expression 2), the term $d\phi_s/d\varepsilon_{\text{LUT}}$ must be calculated and evaluated at $\varepsilon_{\text{REF}}$. Such derivative can be decomposed as

$$\frac{d\phi_s}{d\varepsilon_{\text{LUT}}} = \frac{d\phi_s}{d\varepsilon_{\text{eff}}}\cdot\frac{d\varepsilon_{\text{eff}}}{d\varepsilon_{\text{LUT}}} \tag{14}$$

where $\varepsilon_{\text{eff}}$ is the effective dielectric constant of the sensing line. The first derivative of the right-hand side member in (14) is simply:

$$\frac{d\phi_s}{d\varepsilon_{\text{eff}}} = \frac{\phi_s}{2\varepsilon_{\text{eff}}} \tag{15}$$

as it follows from the fact that

$$\phi_s = \beta l_s = \frac{\omega}{v_p} l_s = \frac{\omega\sqrt{\varepsilon_{\text{eff}}}}{c} l_s \tag{16}$$

$v_p$ being the phase velocity, $c$ the speed of light in vacuum, and $\omega$ the angular frequency.

Concerning the second derivative of the right-hand side member in (14), it can be easily calculated, provided the LUT can be considered semi-infinite in the vertical direction (so that the field lines do not reach the interface of the LUT with the fluidic channel). Under these conditions, the effective dielectric constant is

$$\varepsilon_{\text{eff}} = \frac{\varepsilon_r + \varepsilon_{\text{LUT}}}{2} + \frac{\varepsilon_r - \varepsilon_{\text{LUT}}}{2} F \tag{17}$$

where $\varepsilon_r$ is the substrate dielectric constant and $F$ a geometry factor that depends on the width of the line, $W_s$, and thickness of the substrate, $h$, according to

$$F = \left(1 + 12\frac{h}{W_s}\right)^{-1/2} \tag{18a}$$

provided $W_s > h$. If $W_s < h$, the geometry factor is

$$F = \left(1 + 12\frac{h}{W_s}\right)^{-1/2} + 0.04\left(1 - \frac{W_s}{h}\right)^2 \tag{18b}$$

The validity of (18) requires that $t << h$, as usually occurs, where $t$ is the thickness of the metallic layer. Using (17), the following result is obtained:

$$\frac{d\varepsilon_{\text{eff}}}{d\varepsilon_{\text{LUT}}} = \frac{1}{2}(1 - F) \tag{19}$$

If the semi-infinite approximation is not valid, the effective dielectric constant as a function of the dielectric constant of the LUT must be calculated by any other method, e.g., numerically, or by means of dedicated software tools (e.g., the *ANSYS HFSS* electromagnetic simulator provides the value of $\varepsilon_{\text{eff}}$ from the dielectric constant of the material on top of the line, the transverse geometry of the line, and the height of such material). We should mention at this point that, as it will be later shown, in order to prevent from substrate absorption when a liquid is on top of the sensing line, a protective (dry) film should be used (details of such film will be latter provided). Under these conditions, the semi-infinite approximation (which also requires that the LUT is in direct contact with the sensing line) does not hold, and this will force us to calculate the contribution to the sensitivity given by the last derivative in (14) by means of the *ANSYS HFSS* commercial software and the method specified in Section III.

The contribution to the sensitivity as given by the derivatives in (14) essentially dictates that the sensitivity decreases as the dielectric constant of the REF sample increases [because $\varepsilon_{\text{eff}}$ also increases, and this term appears in the denominator in (15)]. Indeed, many liquids exhibit high dielectric constants, e.g., DI water (with a value of roughly 80). Hence, the typical sensitivities achievable when the REF sample is DI water are low, as compared to those corresponding to solid samples, or other low dielectric constant liquids, such as oils, the LUT materials considered in this work. Indeed, the relevant term to tailor the sensitivity in the limit of small perturbations is (13). Thus, let us next discuss the contribution to the sensitivity given by (13).

In view of (13), depending on the sign of the denominator, the sensitivity can be either positive or negative. If losses are small the terms proportional to $\sinh^2\alpha l_s$ in the denominators of (13) are expected to be small as compared to the terms proportional to $\cosh^2\alpha l_s$, and the sensitivity is negative. We can define a low-loss regime as the one where losses are sufficiently small so as to obtain a negative sensitivity. According to (13a), for $\phi_s = (2n + 1)\cdot\pi/2$, the low-loss regime is thus given by those values of $\alpha$ satisfying $\tanh\alpha l_s < Z_0/Z_s$. Under this regime, the sensitivity is negative, and the magnitude of the sensitivity (its absolute value) increases as $Z_0/Z_s$ decreases. In the lossless limit, with $\alpha = 0$, (13a) is rewritten as

$$\left.\frac{d\phi_\rho}{d\phi_s}\right|_{\phi_s=(2n+1)\cdot\pi/2} = -\frac{2Z_s}{Z_0} \tag{20a}$$

a result identical to the one given in [63], where the sensitivity analysis was performed by excluding losses. Note that the sensitivity goes to infinite in the limiting case where $\tanh \alpha l_s = Z_0/Z_s$. Thus, given a value of $Z_s$, losses might help to boost up the sensitivity [in the absence of losses, by contrast, a high value of $Z_s$ will never bring the sensitivity to extremely high values, as it can be appreciated from expression 20(a)]. For high losses, with $\tanh \alpha l_s > Z_0/Z_s$ (high-loss regime), the phase slope is positive, and the magnitude of the slope increases as $Z_0/Z_s$ increases. For $\phi_s$ = $n\cdot\pi$, the low loss regime is dictated by those values of $\alpha$ satisfying $\tanh \alpha l_s < Z_s/Z_0$, and the sensitivity (negative) exhibits a magnitude that increases as $Z_s/Z_0$ decreases. In the lossless limit, (13b) is rewritten as

$$\left.\frac{d\phi_\rho}{d\phi_s}\right|_{\phi_s=n\cdot\pi} = -\frac{2Z_0}{Z_s} \tag{20b}$$

the value reported in [63]. By contrast, for $\tanh \alpha l_s > Z_s/Z_0$ (high-loss regime), the phase slope is positive and its absolute value increases as $Z_s/Z_0$ increases.

Let us next generalize the sensitivity analysis carried out before by considering an arbitrary number $N$ of impedance inverters. For $N$ even, the input impedance (3) can be rewritten as

$$Z_{in} = Z_{in,s}\cdot\prod_{i=1}^{N} Z_i^{2(-1)^{i+N}} \tag{21}$$

and the reflection coefficient is

$$\rho = \frac{Z_s\dfrac{\sinh 2\alpha l_s - j\sin 2\phi_s}{\cosh 2\alpha l_s - \cos 2\phi_s}\cdot\prod_{i=1}^{N} Z_i^{2(-1)^{i+N}} - Z_0}{Z_s\dfrac{\sinh 2\alpha l_s - j\sin 2\phi_s}{\cosh 2\alpha l_s - \cos 2\phi_s}\cdot\prod_{i=1}^{N} Z_i^{2(-1)^{i+N}} + Z_0} \tag{22}$$

or, alternatively,

$$\rho = \frac{Z_s\dfrac{\sinh 2\alpha l_s - j\sin 2\phi_s}{\cosh 2\alpha l_s - \cos 2\phi_s} - \dfrac{Z_0}{\prod_{i=1}^{N} Z_i^{2(-1)^{i+N}}}}{Z_s\dfrac{\sinh 2\alpha l_s - j\sin 2\phi_s}{\cosh 2\alpha l_s - \cos 2\phi_s} + \dfrac{Z_0}{\prod_{i=1}^{N} Z_i^{2(-1)^{i+N}}}} \tag{23}$$

Formally, expression (23) is identical to expression (7). Namely by replacing $Z_0$ with $Z_0/\prod_{i=1}^{N} Z_i^{2(-1)^{i+N}}$ in (7), expression (23) is obtained. This means that for $N$ even, the derivatives of (13) apply, but replacing $Z_0$ with $Z_0/\prod_{i=1}^{N} Z_i^{2(-1)^{i+N}}$, i.e.,

$$\left.\frac{d\phi_\rho}{d\phi_s}\right|_{\phi_s=(2n+1)\cdot\pi/2} = -\frac{2Z_s\dfrac{Z_0}{\prod_{i=1}^{N} Z_i^{2(-1)^{i+N}}}}{\left(\dfrac{Z_0}{\prod_{i=1}^{N} Z_i^{2(-1)^{i+N}}}\right)^2\cosh^2\alpha l_s - Z_s^2\sinh^2\alpha l_s} \tag{24a}$$

$$\left.\frac{d\phi_\rho}{d\phi_s}\right|_{\phi_s=n\cdot\pi} = -\frac{2Z_s\dfrac{Z_0}{\prod_{i=1}^{N} Z_i^{2(-1)^{i+N}}}}{Z_s^2\cosh^2\alpha l_s - \left(\dfrac{Z_0}{\prod_{i=1}^{N} Z_i^{2(-1)^{i+N}}}\right)^2\sinh^2\alpha l_s} \tag{24b}$$

For $N$ odd, the input impedance (3) is

$$Z_{in} = \frac{\prod_{i=1}^{N} Z_i^{2(-1)^{i+N}}}{Z_{in,s}} \tag{25}$$

and the reflection coefficient is

$$\rho = \frac{\dfrac{\prod_{i=1}^{N} Z_i^{2(-1)^{i+N}}}{Z_s\dfrac{\sinh 2\alpha l_s - j\sin 2\phi_s}{\cosh 2\alpha l_s - \cos 2\phi_s}} - Z_0}{\dfrac{\prod_{i=1}^{N} Z_i^{2(-1)^{i+N}}}{Z_s\dfrac{\sinh 2\alpha l_s - j\sin 2\phi_s}{\cosh 2\alpha l_s - \cos 2\phi_s}} + Z_0} \tag{26}$$

or, alternatively,

$$\rho = -\frac{Z_s\dfrac{\sinh 2\alpha l_s - j\sin 2\phi_s}{\cosh 2\alpha l_s - \cos 2\phi_s} - \dfrac{\prod_{i=1}^{N} Z_i^{2(-1)^{i+N}}}{Z_0}}{Z_s\dfrac{\sinh 2\alpha l_s - j\sin 2\phi_s}{\cosh 2\alpha l_s - \cos 2\phi_s} + \dfrac{\prod_{i=1}^{N} Z_i^{2(-1)^{i+N}}}{Z_0}} \tag{27}$$

Except by the (–) sign, expression (27) is identical to (7), provided $Z_0$ is replaced with $\prod_{i=1}^{N} Z_i^{2(-1)^{i+N}}/Z_0$. Since the (–) sign in (27) introduces a constant phase of π, the derivatives of (13) also apply for $N$ odd, but in this case by replacing $Z_0$ with $\prod_{i=1}^{N} Z_i^{2(-1)^{i+N}}/Z_0$. Thus, the following derivatives are obtained:

$$\left.\frac{d\phi_\rho}{d\phi_s}\right|_{\phi_s=(2n+1)\cdot\pi/2} = -\frac{2Z_s\dfrac{\prod_{i=1}^{N} Z_i^{2(-1)^{i+N}}}{Z_0}}{\left(\dfrac{\prod_{i=1}^{N} Z_i^{2(-1)^{i+N}}}{Z_0}\right)^2\cosh^2\alpha l_s - Z_s^2\sinh^2\alpha l_s} \tag{28a}$$

$$\left.\frac{d\phi_\rho}{d\phi_s}\right|_{\phi_s=n\cdot\pi} = -\frac{2Z_s\dfrac{\prod_{i=1}^{N} Z_i^{2(-1)^{i+N}}}{Z_0}}{Z_s^2\cosh^2\alpha l_s - \left(\dfrac{\prod_{i=1}^{N} Z_i^{2(-1)^{i+N}}}{Z_0}\right)^2\sinh^2\alpha l_s} \tag{28b}$$

With $N$ = 0, it was shown before that the limit between the low-loss and the high-loss regime is dictated by the ratio $Z_s/Z_0$, particularly, for $\phi_s$ = $(2n + 1)\cdot\pi/2$, the low-loss regime corresponds to values of $\alpha$ satisfying $\tanh \alpha l_s < Z_0/Z_s$, and $\tanh \alpha l_s > Z_0/Z_s$ for the high-loss regime, whereas for $\phi_s$ = $n\cdot\pi$, the low loss regime is dictated by those values of $\alpha$ satisfying $\tanh \alpha l_s < Z_s/Z_0$, and $\tanh \alpha l_s > Z_s/Z_0$ for high losses. The same applies when $N \neq 0$, but replacing $Z_0$ with $Z_0/\prod_{i=1}^{N} Z_i^{2(-1)^{i+N}}$ for $N$ even, and replacing $Z_0$ with $\prod_{i=1}^{N} Z_i^{2(-1)^{i+N}}/Z_0$ for $N$ odd.

Let us next summarize the strategy for sensitivity enhancement in the limit of small perturbations when $N$ is an arbitrary number:

- Case A: $\phi_s = (2n + 1)\cdot\pi/2$. In the low-loss regime, $Z_s$ must be as high as possible. For $N$ even, $Z_0/\prod_{i=1}^{N} Z_i^{2(-1)^{i+N}}$ must be as low as possible, and for $N$ odd, $\prod_{i=1}^{N} Z_i^{2(-1)^{i+N}}/Z_0$ must be as low as possible, in both cases ensuring that the denominators of 24(a) and 28(a) are positive, as corresponds to the low-loss regime. In both cases ($N$ even and odd) the characteristic impedance of the inverter cascaded to the sensing line, $Z_1$, must be low, and the subsequent inverter impedances must by high and low, alternating. This is the most usual operation mode. However, for certain materials, such as liquids, with high level of losses, operation in the high-loss regime is possible. For the high-loss regime, sensitivity optimization occurs when the denominator of (24a), for $N$ even, and the denominator of (28a), for $N$ odd, are close to zero and negative. Thus, under this operation regime, the sensitivity increases when $Z_0/Z_s \prod_{i=1}^{N} Z_i^{2(-1)^{i+N}}$ increases for $N$ even, and when $\prod_{i=1}^{N} Z_i^{2(-1)^{i+N}}/Z_0\, Z_s$ increases for $N$ odd.
- Case B: $\phi_s = n\cdot\pi$. In the low-loss regime, $Z_s$ must be as low as possible. For $N$ even, $Z_0/\prod_{i=1}^{N} Z_i^{2(-1)^{i+N}}$ must be as high as possible, and for $N$ odd, $\prod_{i=1}^{N} Z_i^{2(-1)^{i+N}}/Z_0$ must be as high as possible, in both cases ensuring that the denominators of 24(b) and 28(b) are positive, as corresponds to the low-loss regime. In both cases ($N$ even and odd), the characteristic impedance of the inverter in contact with the sensing line must be high, and the additional cascaded inverters (if they are present) must exhibit a characteristic impedance with low and high values alternating. For the high-loss regime, the sensitivity increases when $Z_s \prod_{i=1}^{N} Z_i^{2(-1)^{i+N}}/Z_0$ increases for $N$ even, and when $Z_s Z_0/\prod_{i=1}^{N} Z_i^{2(-1)^{i+N}}$ increases for $N$ odd.

In summary, the overall sensitivity in the limit of small perturbations for the sensor with $N$ inverters terminated with either an open-ended half-wavelength or an open-ended quarter-wavelength sensing resonator is given by:

$$S = \frac{d\phi_\rho}{d\phi_s}\cdot\frac{d\phi_s}{d\varepsilon_{\mathrm{LUT}}} = \frac{d\phi_\rho}{d\phi_s}\cdot\frac{d\phi_s}{d\varepsilon_{\mathrm{eff}}}\cdot\frac{d\varepsilon_{\mathrm{eff}}}{d\varepsilon_{\mathrm{LUT}}} \tag{29}$$

where the last two terms are given by (14), (15), and (19), and the first term is given by (13) for $N = 0$, by (24) for $N$ even and by (28) for $N$ odd.

It should be mentioned that a variation in the phase of the reflection coefficient can also be caused by a change in the loss tangent of the LUT, $\tan\delta_{\mathrm{LUT}}$, since $\tan\delta_{\mathrm{LUT}}$ is intimately related with the attenuation constant, $\alpha$ [see expressions (9) and (10)]. Usually, a variation of the dielectric constant of the LUT, $\varepsilon_{\mathrm{LUT}}$, in the vicinity of the REF value, $\varepsilon_{\mathrm{REF}}$, is accompanied with a variation in $\tan\delta_{\mathrm{LUT}}$, or $\alpha$. However, the derivative of $\phi_\rho$ with $\alpha$ is null in the limit of small perturbations, and for this reason the effects of $\tan\delta_{\mathrm{LUT}}$ variation have been ignored. This aspect is demonstrated in Appendix A.

## III. The Proposed Liquid Sensors and Validation of the Sensitivity Analysis

Three prototype sensors have been designed and fabricated. In all cases, the sensing line is an open-ended quarter-wavelength transmission line. The difference concerns the number $N$ of impedance inverters and the operation regime. Thus, in the so-called sensor A, a single inverter is cascaded to the sensing line ($N = 1$), and the sensor operates under the low-loss regime. Sensor B utilizes two inverters ($N = 2$) and operates under the high-loss regime. Finally, sensor C uses two inverters ($N = 2$) with an optimized value of the impedance of the second one ($Z_2$) to boost up the sensitivity in the limit of small perturbations (it operates in the low-loss regime). The main aim of this section is to validate the previous sensitivity analysis on the basis of the three designed and fabricated prototype sensors. It is considered that the REF liquid is sunflower oil with measured dielectric constant and loss tangent of $\varepsilon_{\mathrm{REF}} = 2.6$ and $\tan\delta_{\mathrm{REF}} = 0.065$ at the operation frequency of the sensor ($f_0$) and at room temperature (22ºC). In the considered sensors, the liquid samples (different types of oils in all cases) are put in contact with the sensing line by means of a fluidic channel made of methacrylate (with estimated dielectric constant of 2.4). The height of such channel is 3 mm, the width is 50 mm, and the length extends from the contact plane between the sensing line and the first cascaded impedance inverter up to a distance beyond the open-end of the sensing line (the total length being 25.35 mm). Moreover, in order to prevent from substrate absorption, we have coated the sensing region with a dry film of PET (Polyethylene Terephthalate), with a thickness of 0.06 mm and an estimated dielectric constant and dielectric loss tangent of 3.5 and 0.01 respectively.

Before designing the sensors, we have first estimated the attenuation constant, $\alpha$, when the fluidic channel contains the REF oil ($\alpha$ is a relevant parameter for the theoretical prediction of the sensitivity in the limit of small perturbations). For that purpose, we have carried out the electromagnetic simulation of the reflection coefficient of the open-ended 90º sensing line. The considered length of that line is $l_s = 20.7$ mm, whereas its width is $W_s = 0.2$ mm. With such width, the characteristic impedance of the sensing line with the fluidic channel loaded with the REF oil is $Z_s = 134.72\ \Omega$ (the effects of the dry film and methacrylate have been taken into account). The considered substrate is the *Rogers 4003C* with dielectric constant $\varepsilon_r = 3.55$, thickness $h = 1.524$ mm, and loss factor $\tan\delta = 0.0022$. Figure 2 depicts the reflection coefficient, represented in the Smith Chart, seen from the input port of the sensing line. At resonance, i.e., for $\phi_s = 90$º, the reflection coefficient (8) is a real number given by

$$\rho = \frac{Z_s \sinh 2\alpha l_s - Z_0\,(\cosh 2\alpha l_s + 1)}{Z_s \sinh 2\alpha l_s + Z_0\,(\cosh 2\alpha l_s + 1)} \tag{30}$$

Note that if losses are absent, $\rho = -1$, corresponding to a short circuit seen from the input port (the 90º line inverts the open-end termination of the line). The effect of losses is a displacement of the reflection coefficient at resonance slightly to the right in the Smit Chart. Since $Z_s$ is known, and $Z_0$ = 50 Ω, from the (real) value of $\rho$ at resonance (given by the cross of the trace of $\rho$ in the Smith Chart with the horizontal axis), the value of $\alpha$ can be inferred. The resonance frequency (where $\phi_s = 90º$) can be accurately determined, since it is the frequency corresponding to the cross of $\rho$ in the Smith Chart with the horizontal axis. Since $l_s$ is known, the phase constant, $\beta$, and the phase velocity can be obtained, and from the phase velocity, the effective dielectric constant can be retrieved [see (16)]. Note that the effective dielectric constant does not appear in (13), (24) or (28). However, for the calculation of the overall sensitivity, the last term in (29) is necessary, and (19) does not apply. Consequently, we can apply the previous method for the determination of the effective dielectric constant as a function of the dielectric constant of the LUT, and from this dependence we can obtain the last term in (29). Namely, for each $\varepsilon_{LUT}$ value in the vicinity of $\varepsilon_{REF}$, we can represent the reflection coefficient in the Smith chart, and determine the frequency where the trace crosses the horizontal axis. Once this frequency is determined, $\varepsilon_{eff}$ can be inferred using (16). Note also that $\varepsilon_{eff}$ is necessary for the calculation of $d\phi_s/d\varepsilon_{\text{eff}}$ in (29), as given by (15). An alternative to this method to retrieve $\varepsilon_{\text{eff}}$ (or $d\varepsilon_{\text{eff}}/d\varepsilon_{\text{LUT}}$) is to use the *ANSYS HFSS* commercial software, which is able to directly provide $\varepsilon_{\text{eff}}$ (or $d\varepsilon_{\text{eff}}/d\varepsilon_{\text{LUT}}$) from the transverse geometry (sensor substrate, dry film, and LUT) and material parameters (dielectric constants and loss tangents). In this paper, we have used this latter approach providing a value for $\varepsilon_{\text{eff}}$ and $d\varepsilon_{\text{eff}}/d\varepsilon_{\text{LUT}}$ of 3.10 and 0.28, respectively.

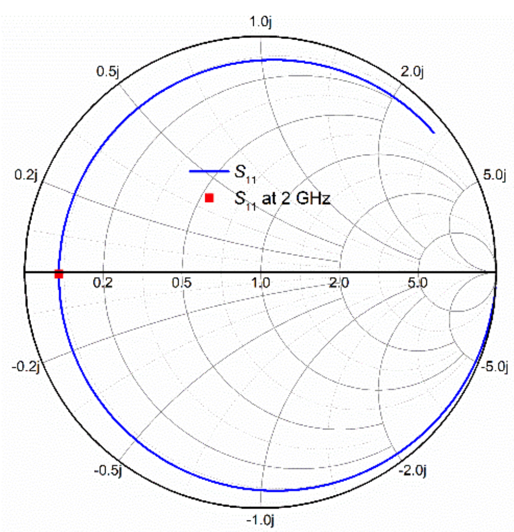


**Fig. 2.** Representation of the reflection coefficient in the Smith Chart, as inferred from full wave electromagnetic simulation for the sensing line with dimensions indicated in the text and coated with a material with the dielectric characteristics of sunflower oil (see text), fluidic holder and PET film.

With the estimated value of $\alpha$ (= 0.967 Np/m), the derivative (13a) is found to be –5.40 and the overall sensitivity using (29) is found to be $S_{th}$ = – 22.02º (note that this is the sensitivity in the limit of small perturbations). The absolute value of such sensitivity is slightly superior to the one achieved by excluding losses, since, in this case, the derivative of 13(a), which reduces to 20(a), is –5.36. Although the sensor merely based on the sensing line ($N = 0$) has not been fabricated, we have obtained the dependence of $\phi_\rho$ with $\varepsilon_{LUT}$ from full wave electromagnetic simulation (the loss tangent has been set to $\tan\delta_{\text{REF}}$ = 0.065). The results are depicted in Fig. 3. From these simulated data points, the derivative has been obtained (also depicted in Fig. 3), and the value corresponding to $\varepsilon_{LUT} = \varepsilon_{REF}$ ($S_{sim}$ = –23.73º) is in good agreement with the theoretical prediction.

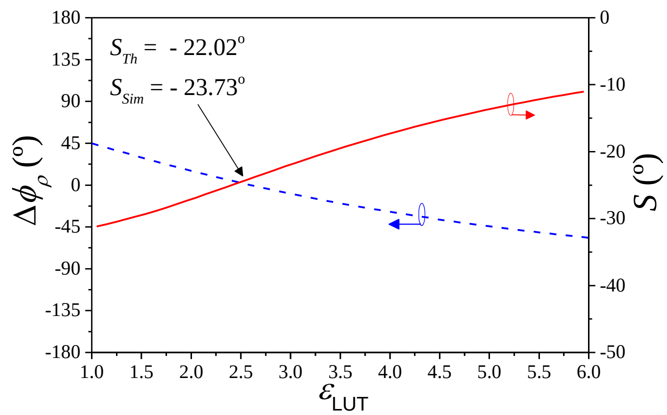


**Fig. 3.** Variation of $\phi_\rho$ with $\varepsilon_{LUT}$ for the considered open-ended quarter-wavelength sensing line, and sensitivity. The operating frequency is $f_0$ = 2 GHz.

### *A. Prototype Sensor A (N = 1 and operation in the low-loss regime)*

Based on the previous sensing line, the first fabricated one-port phase-variation liquid sensor (sensor A) has been implemented by cascading a single impedance inverter ($N$ = 1) with low characteristic impedance ($Z_1$ = 24.64 Ω) to such line. The width and length of such cascaded transmission line section is $W_1$ = 9.1 mm and $l_1$ = 21.72 mm, respectively, corresponding to a low-impedance quarter-wavelength transmission line section. Figure 4 depicts the top view of the microwave structure (sensing line, impedance inverter and access line), as well as a photograph of the whole sensor, which includes the fluidic channel, and fluidic connectors. The microwave part has been fabricated by means of the *LPKF HF100* drilling machine.

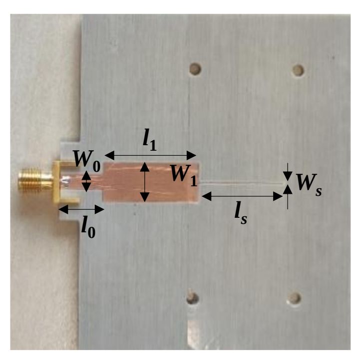


(a)

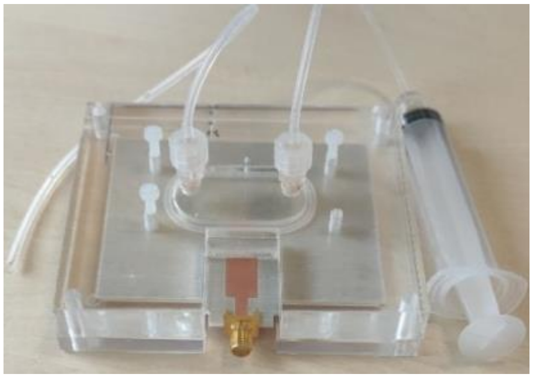

(b)

**Fig. 4.** Photograph of the fabricated sensor with $N$ = 1 (sensor A). (a) Top view of the microwave module; (b) complete sensor. Dimensions (in mm) are: $W_0$ = 3.4, $l_0$ = 10.0, $W_1$ = 9.1, $l_1$ = 21.72, $W_s$ = 0.20, and $l_s$ = 20.7.

With the value of $\alpha$ found before and the characteristic impedances of the sensing line and inverter, expression (28a) (the one that should be applied for $N$ odd) gives –25.93, a value substantially superior (in absolute value) than the one obtained when a single sensing line is considered. The (–) sign means that the sensor operates under the low-loss regime. The whole sensitivity in the limit of small perturbations, given by (29), is found to be $S_{th}$ = –105.75º. We have obtained the sensor response (dependence of $\phi_\rho$ with $\varepsilon_{\rm LUT}$) through electromagnetic simulation (we have excluded the effects of the access line). The considered loss tangent is the one of the REF liquid ($\tan\delta_{\rm REF}$ = 0.065), and it is assumed that it does not change with $\varepsilon_{\rm LUT}$. The results are depicted in Fig. 5. Such figure includes also the sensitivity inferred from the simulated data points. The sensitivity in the limit of small perturbations ($\varepsilon_{\rm LUT} = \varepsilon_{\rm REF}$) is found to be $S_{sim}$ = –101.70º, in reasonably good agreement with the theoretical value.

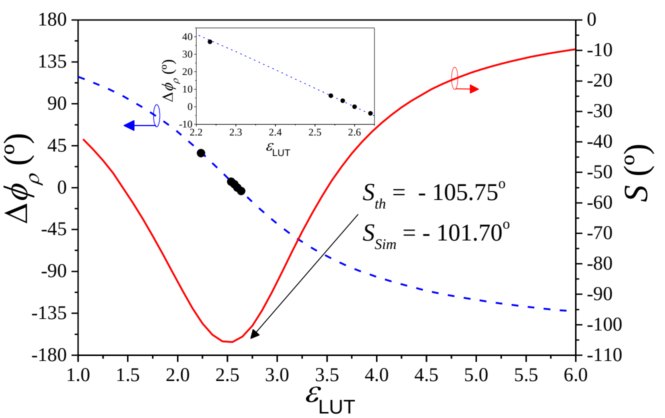


**Fig. 5.** Variation of $\phi_\rho$ with $\varepsilon_{\rm LUT}$ for the considered liquid sensor A with $N$ = 1, and sensitivity. The operating frequency is $f_0$ = 1.980 GHz. The dots correspond to the measured phases with different LUTs (oils). The dielectric constant values inferred with the proposed sensor are 2.235 (motor oil) 2.540 (olive oil), 2.600 (sunflower oil), 2.570 (sesame oil), and 2.640 (coconut oil), whereas those obtained with the dielectric probe are 2.239 (motor oil), 2.550 (olive oil), 2.600 (sunflower oil), 2.590 (sesame oil), and 2.730 (coconut oil). A zoom of the region of interest with the measured data is included as an inset.

We have used the fabricated sensor of Fig. 4 to infer the response of different types of oils. The measured phase responses (at $f_0$) are included in Fig. 5, particularly, at the corresponding phase value inferred from simulation. From these data, the dielectric constant of the different oils has been obtained (given by the anti-image value), and the agreement with independent measurements carried out by means of the *DAK-3.5 R140B* dielectric probe is good (see the values in the caption of Fig. 5).

### *B. Prototype Sensor B (N = 2 and operation in the high-loss regime)*

Increasing the number $N$ of inverter stages eases operation in the high-loss regime. To verify this, let us carefully analyze the denominators of expressions (24a) and (28a), corresponding to $N$ even and $N$ odd, respectively, and for a quarter-wavelength (or odd multiple) sensing line, the case under consideration. In both cases, as the number of inverter stages ($N$) increases, the weighting term of $\cosh^2\alpha l_s$ in the denominators ($Z_0/\prod_{i=1}^{N} Z_i^{2(-1)^{i+N}}$ for $N$ even and $\prod_{i=1}^{N} Z_i^{2(-1)^{i+N}}/Z_0$ for $N$ odd) decreases, provided $Z_1$ is low, $Z_2$ is high, $Z_3$ is low, and so on. Thus, given a certain level of losses (dictated by $\alpha$), the likelihood that the sensor operates under the high-loss regime is higher if $N$ is high [this occurs when the denominator in expressions (24) and (28) is negative]. Indeed, for $N$ = 2, and an appropriate selection of the inverter impedances, operation in the high-loss regime can be easily achieved (to be discussed next).

The second designed and fabricated liquid sensor (designated as sensor B), with $N$ = 2, is depicted in Fig. 6. The dimensions of the sensing line and inverter line 1 are identical to those of the previous sensor. The second inverter line exhibits a characteristic impedance of $Z_2$ = 156.14 Ω, and the width and length of such quarter-wavelength transmission line section is $W_2$ = 0.2 mm and $l_2$ = 23.85 mm, respectively. With the characteristic impedances of the sensing line and inverters, expression (24a) (the one that should be applied for $N$ even) gives +50.98, a positive value. Consequently, the sensor operates under the high-loss regime. The whole sensitivity in the limit of small perturbations, given by (29), is found to be $S_{th}$ = +207.88º. The dependence of $\phi_\rho$ with $\varepsilon_{\rm LUT}$, as inferred through electromagnetic simulation (excluding the effects of the access line), is depicted in Fig. 7. Similar to Fig. 5, the considered loss tangent is the one of the REF liquid, and it is assumed that it does not change with $\varepsilon_{\rm LUT}$. The sensitivity, inferred from the simulated data points, also included in the figure, reveals that, in the limit of small perturbations ($\varepsilon_{\rm LUT} = \varepsilon_{\rm REF}$), the value ($S_{sim}$ = +206.66º) is in good agreement with the theoretical value.

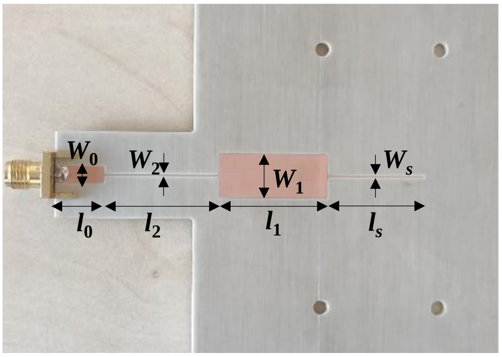


(a)

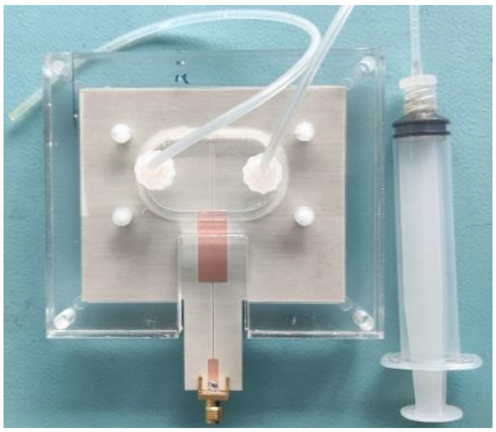

(b)

**Fig. 6.** Photograph of the fabricated sensor B with $N = 2$. (a) Top view of the microwave module; (b) complete sensor. Dimensions (in mm) are: $W_0 = 3.4$, $l_0 = 10.0$ , $W_2 = 0.2$, $l_2 = 23.89$, $W_1 = 9.1$, $l_1 = 21.72$, $W_s = 0.2$, and $l_s = 20.7$.

The same oils used to verify the functionality of the previous sensor have been the considered LUTs in the sensor of Fig. 6. The measured phase responses (at $f_0$) are included in Fig. 7, and the dielectric constants of the different oils are given in the caption of that figure. Again, the agreement with the measurements carried out by means of the *DAK-3.5 R140B* dielectric probe is good. Notice that in this case (Fig. 7), the dielectric constant of motor oil (2.239) cannot be extracted by measuring the phase variation of $\phi_\rho$ since the dynamic range of operation (where the phase slope is positive – high loss regime) is limited. Typically, when losses are significant, the sensor response (dependence of $\phi_\rho$ with $\varepsilon_{LUT}$) no longer exhibits a monotonic variation. Rather than that, a bi-valued dielectric constant for each phase point appears in certain regions, and, under these circumstances, the sensor functionality is no longer valid. This aspect has been verified by means of electromagnetic simulation, by considering the sensor of Fig. 6, but with the phase response parametrized by the loss tangent of the LUT. These phase responses are depicted in Fig. 8, where it can be appreciated that, in some cases, the response is non-monotonic. Thus, when operating in the high-loss regime, the input dynamic range should be circumscribed to a very small region in the vicinity of the REF dielectric constant.

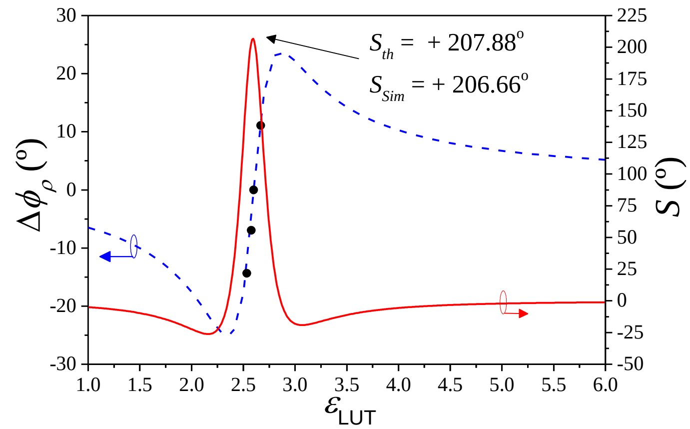


**Fig. 7.** Variation of $\phi_\rho$ with $\varepsilon_{LUT}$ for the considered liquid sensor B with $N = 2$, and sensitivity. The operating frequency is $f_0 = 1.980$ GHz. The dots correspond to the measured phases with different LUTs (oils). The dielectric constant values inferred with the proposed sensor are 2.535 (olive oil), 2.600 (sunflower oil), 2.578 (sesame oil), and 2.670 (coconut oil), whereas those obtained with the dielectric probe are 2.550 (olive oil), 2.600 (sunflower oil), 2.590 (sesame oil), and 2.730 (coconut oil).

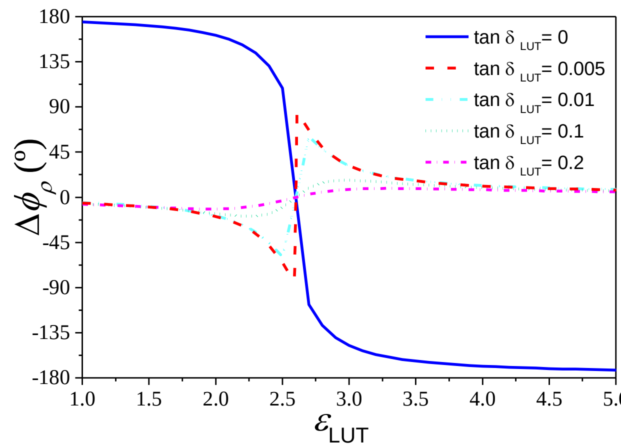


**Fig. 8.** Variation of $\phi_\rho$ with $\varepsilon_{LUT}$ for the considered liquid sensor with $N = 2$, parametrized by the loss tangent of the LUT, $\tan\delta_{LUT}$.

The non-monotonic phase response might also occur in situations where a change in the dielectric constant of the LUT leads also to a change in the loss tangent. For example, in binary mixtures of liquids with unequal (and very different) dielectric constants and loss tangents, a change in the volume fraction is expected to generate significant changes in both the dielectric constant and the loss tangent. Under these conditions, a non-monotonic response (even, but not necessarily, caused by a change of regime) is more likely to occur. Nevertheless, it should be mentioned that the interest in highly sensitive liquid sensors concerns the measurement and detection of small changes in the properties of the LUT. If the input dynamic range is limited, then it is possible to design the sensor to operate within the monotonic range (and avoid a change of regime).

### C. *Prototype Sensor C (N = 2 and operation in the low-loss regime)*

The sensitivities obtained in sensors A and B in the limit of small perturbations are good. Such sensitivities can be further improved, especially for the sensor with $N = 2$ (with more degrees of freedom), by appropriately choosing the impedances of the inverters. Namely, the sensitivity increases dramatically in the limit when the denominators of expressions (24) and (28) are null, and such limit is more easily achievable if more than one inverter stage is considered. Let us next consider the topology of the sensor in Fig. 6 (i.e., a liquid sensor with $N = 2$), where the characteristic impedance, $Z_s$, and length, $l_s$, of the sensing line, as well as the characteristic impedance, $Z_1$, and length, $l_1$, of the first inverter are maintained. It is possible to increase the sensitivity in the limit of small perturbations of $\varepsilon_{LUT}$ by modifying only the value of the characteristic impedance of inverter 2, $Z_2$. According to equation (24a), by setting the characteristic impedance of such inverter to $Z_2 = 83.16\ \Omega$ (considering air on top of it and the same length $l_2$), the sensor exhibits a low-loss regime of operation, at least in the limit of small perturbations. With the new characteristic impedances of inverter 2, $Z_2$, expression (24a), the one that should be applied for $N$ even, gives –105.11, a negative value. In this case, the variation of $\phi_\rho$ with $\varepsilon_{LUT}$ (inferred by electromagnetic simulation) for the considered optimized liquid sensor with $N = 2$ (Fig. 9) is shown in Fig. 10.

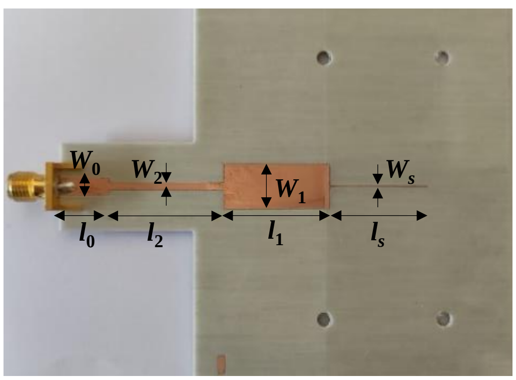


**Fig. 9.** Photograph of the fabricated optimized sensor C with $N = 2$. Dimensions (in mm) are: $W_0 = 3.4$, $l_0 = 10.0$, $W_2 = 1.33$, $l_2 = 23.25$, $W_1 = 9.1$, $l_1 = 21.72$, $W_s = 0.2$, and $l_s = 20.7$.

The whole sensitivity in the limit of small perturbations, given by (29), is found to be $S_{th} = –507.05°$ (2.46 times higher than the sensitivity of the sensor B of Fig. 6 with the same dimensions for the whole sensor). Again, the same set of oil samples used in the previous prototypes has been tested to verify the functionality of the optimized sensor C. The measured phase variation of the reflection coefficient at $f_0$ is plotted with black dots in Fig. 10. The extracted dielectric constants of the different measured oils are listed in the caption of the figure. Besides increasing the sensitivity for small perturbations around the REF dielectric constant (the dielectric constant of sunflower oil) without increasing overall sensor dimensions, the device exhibits operation in the low-loss regime, and the dielectric constant of motor oil can be (again) fully characterized (note that the response is monotonic). The sensitivity, inferred from the simulated data points (excluding the effect of the access line) is included in the figure, and reveals that, in the limit of small perturbations ($\varepsilon_{LUT} = \varepsilon_{REF}$), the value ($S_{sim} = –502.80°$) is in good agreement with the theoretical value. Such high sensitivity is aided by losses, as reveals the fact that (24a) reduces to –67.56 when losses are excluded (note that the value is –105.11 when losses are considered, as indicated in the preceding paragraph).

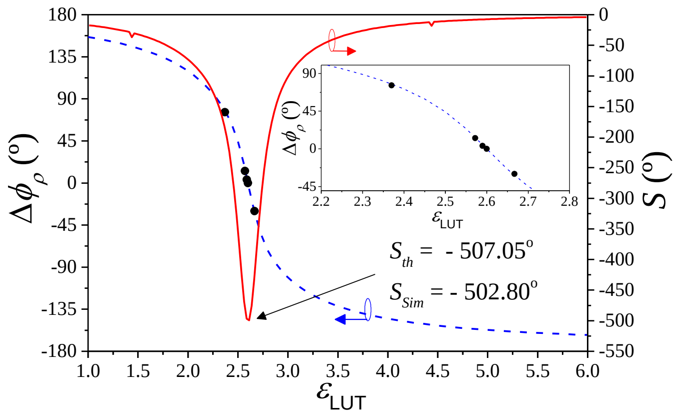


**Fig. 10.** Variation of $\phi_\rho$ with $\varepsilon_{LUT}$ for the considered liquid sensor C with $N = 2$, and sensitivity. The operating frequency is $f_0 = 1.980$ GHz. The dots correspond to the measured phases with different LUTs (oils). The dielectric constant values inferred with the proposed sensor are 2.376 (motor oil) 2.570 (olive oil), 2.600 (sunflower oil), 2.590 (sesame oil), and 2.667 (coconut oil), whereas those obtained with the dielectric probe are 2.239 (motor oil), 2.550 (olive oil), 2.600 (sunflower oil), 2.590 (sesame oil), and 2.730 (coconut oil). A zoom of the region of interest with the measured data is included in the inset.

*D. Application to the Characterization of Edible Oils by Usage*

In the final experiment reported in the present paper, the highly sensitive sensor C of Fig. 9 has been used to detect the changes experienced by an edible sunflower oil by usage (in frying processes). The nominal dielectric constant of such (unfried) oil is $\varepsilon_{LUT} = \varepsilon_{REF} = 2.6$. Thus, this experiment is of particular interest to analyze the capability of sensor C to detect very tiny changes in the dielectric properties of the LUT. For that purpose, we have fried potatoes (150 g of fresh potatoes) in cycles of 10 minutes at 185 ºC. An oil sample (of roughly 10 mL) has been obtained and cooled down for 30 min after the different frying cycles for characterization. The measured responses for the different oil samples are depicted in Fig. 11. The sensor is able to capture the changes experienced by the oil due to its usage, mainly caused by the accumulation of water. Figure 12 depicts the phase of the reflection coefficient at $f_0$, referred to the phase of the unused oil, as a function of the number of frying cycles. The phase varies roughly linearly, and the average sensitivity is found to be 24.63º per frying cycle. These results point out that the designed and fabricated sensor C of Fig. 9 is very sensitive and can be used to detect the deterioration-related dielectric changes experienced by edible oil, when it is subjected to repeated frying cycles.

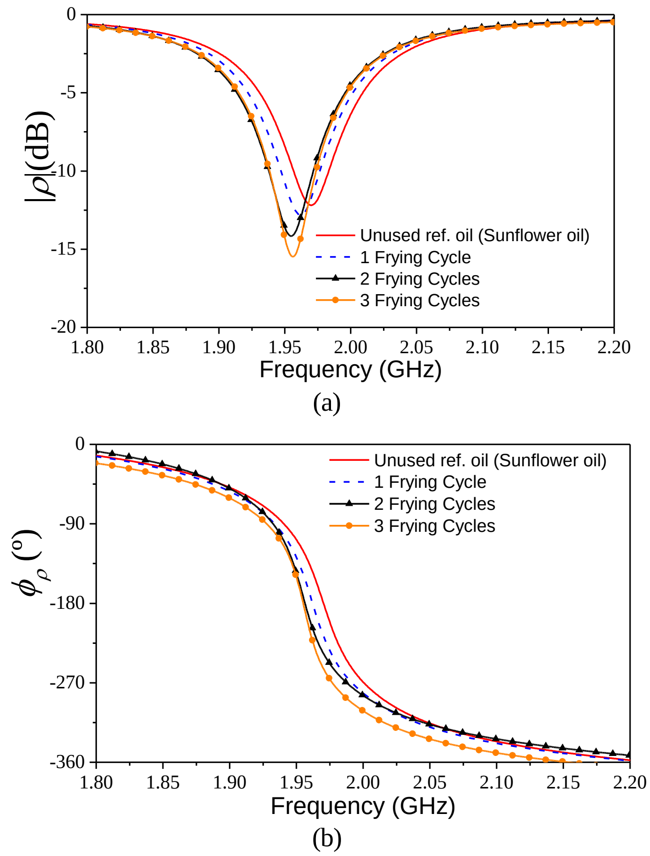


**Fig. 11.** Measured frequency response of the sensor C of Fig. 9 loaded with unused oil and with oils subjected to different frying cycles (indicated in the figure). (a) Magnitude response; (b) phase response.

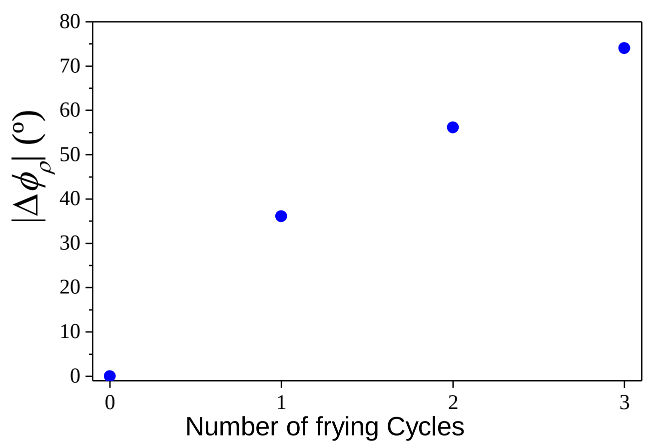


**Fig. 12.** Dependence of the phase (in absolute value) of the reflection coefficient at $f_0$ with the number of frying cycles for the sensor of Fig. 9.

## IV. Discussion and Comparison

Most reported phase-variation sensors, either operating in reflection or in transmission, are devoted to the characterization of solid samples [56], [57], [59]-[61], [63]-[67], [69]-[72]. Exceptions are the differential transmission-mode sensor reported in [58], based on a pair of meander lines, and the reflective-mode submersible sensor of ref. [73], based on the same topology as the sensors of this work, and focused on the determination of ethanol concentration in deionized (DI) water. In such latter sensor, the sensitivity is moderate, as compared to the sensitivities achieved in the sensors of this work, or to the sensitivities of other phase-variation sensors aimed to the analysis of solid samples. The main reason that explains the limited sensitivity in the sensor of [73] is the fact that the considered REF liquid is DI water, with a dielectric constant of roughly $\varepsilon_{REF}$ = 80 at the operating frequency of the sensor. This high dielectric constant value provides also a high effective dielectric constant of the sensing line, $\varepsilon_{eff}$, which appears in the denominator in (15), and thereby degrades the sensitivity. Moreover, in the submersible sensor of [73], a 60-μm protective dry film of polyethylene terephthalate (PET) was used to prevent from substrate absorption. Such dry film further degrades the sensitivity (despite its small thickness), since many electric field lines generated by the sensing line are concentrated in such layer. In the sensors of Figs. 4 (Sensor A), 6 (sensor B), and 9 (sensor C), a dry film is also used, thereby limiting the sensitivity. However, the dielectric constant of the considered REF oil is more than one order of magnitude lower than the one of DI water. Consequently, the achievable sensitivity with one ($N$ = 1) or two ($N$ = 2) inverter stages is by far superior to the one of the submersible sensor of [73], and comparable to the one of other reflective-mode phase-variation sensors devoted to the measurement of the dielectric properties of solids.

Table I compares the sensitivity and other sensor parameters of various reported phase-variation sensors, in particular the main figure of merit (FoM), defined as the ratio between the maximum sensitivity and the area of the sensing region expressed in terms of the squared guided wavelength ($\lambda_g^2$). The performance of the proposed liquid sensors is comparable to the one of other sensors (for solids) that appear in Table I (note that the table reports the characteristics of Sensor C, only). The sensitivity can be enhanced by adding further inverters, or by conveniently adjusting the impedances of the inverters and sensing line [note that in the limit when the denominators in (24) and (28) are null, the sensitivity dramatically increases]. Nevertheless, the main objective of this paper has been to analyze the effects of MUT losses on sensitivity, and we have considered oils, since these substances are lossy samples, very useful to validate the main conclusions derived from the analysis.

On the other hand, in order to demonstrate the potential of one of the proposed sensors to detect small changes in the dielectric properties of the MUT, we have modified the dielectric properties of an edible oil by usage (by subjecting it to multiple frying cycles), and the sensor has been able to discriminate different states of oil degradation (as revealed by the varying phase of the reflection coefficient at the operating frequency). There are many different techniques for the characterization of used oils, including luminescence spectroscopy [75], dielectric spectroscopy [76], [77], impedance spectrometry [78], electrical impedance sensing [79], capacitive sensing [80]-[82], and machine vision systems [83], among others. However, microwave technologies offer low-cost solutions for sensing, and such technologies oriented towards the characterization of oils, and in general towards food quality assessment, have been a subject of research in recent years. Thus, in [84]-[87], oil sensors based on semi-lumped resonators have been proposed. However, the working principle in such sensors is the variation in the resonance frequency (and eventually magnitude) of the notch or peak, caused by the changes in the dielectric properties of the oil samples, when they are subjected to frying processes. Therefore, a faithful quantitative comparison with the sensors reported in this work (with a completely different working principle) is not possible, and, for that reason, such sensors are not included in Table I (only devoted to phase-variation sensors). Nevertheless, a qualitative comparison is reasonable to be discussed in the next paragraph.

TABLE I
COMPARISON OF VARIOUS PHASE-VARIATION SENSORS

| **Ref.** | **Mode** | **Sensing size* ($\lambda_g^2$)** | **Overall size ($\lambda_g^2$)** | **Max. Sensitivity** | **FoM (º/$\lambda_g^2$)** |
|---|---|---|---|---|---|
| [63] | RX | 0.025 | 0.131 | 528.7º | 21148 |
| [64] | RX | 0.100 | 0.297 | 45.5º | 455 |
| [54] | TX | --- | --- | 600 dB | --- |
| [55] | TX | --- | --- | 54.8º | --- |
| [56] | TX | 12.90 | 12.90 | 415.6º | 32.2 |
| [57] | TX | 0.075 | 0.075 | 25.3 dB | --- |
| [58] | TX | 0.020 | 0.40 | 17.6 dB | --- |
| [65] | RX | 0.065 | 0.126 | 101.3º | 1558 |
| [59] | TX | 0.030 | 0.090 | 7.7º | 257 |
| [60] | TX | 0.040 | 0.054 | 20.0º | 500 |
| [61] | TX | 0.038 | 0.053 | 12.3º | 332 |
| [66] | RX | 0.015 | 0.073 | 83.35º | 5643 |
| [67] | RX | 0.018 | 0.076 | 66.5º | 3643 |
| [69a] | RX | 0.070 | 0.070 | 659.6º | 9401 |
| [69b] | RX | 0.058 | 0.058 | 736.0º | 12690 |
| [70] | RX | 0.017 | 0.103 | 468.0º | 27419 |
| [73] | RX | 0.023 | 0.032 | 1.00º | 865.05 |
| **T.W. sensor C** | **RX** | **0.0286** | **0.092** | **502.8º** | **17551º** |

*This size corresponds to the sensing region, not to the size of the whole sensing structure, referred to as overall size and indicated in the adjacent column to the right.

For example, the sensor in [85] is a one-port reflective-mode sensor acting as a planar submersible probe loaded with a pair of complementary split ring resonators (CSRRs). The output variable is the resonance in the reflection coefficient, dictated by the dielectric properties of the considered oil sample. In such sensor, deterioration of an edible oil is emulated by the adulteration with mineral oil, and it is reported that the minimum deducible frequency shift corresponding to 10% adulteration of mineral oil in the edible oil is found to be approximately 14 MHz. This resolution does not seem to be comparable to the one of the proposed sensors, able to detect tiny changes caused by the frying processes. The sensor in [86], also resonant, operates in transmission and reflection, and can detect the changes generated in an edible sunflower oil by usage (by frying potatoes, similar to this work), through the changes in the resonance frequency. It is reported that changes in the dielectric constant of the fried oil between 2.9 and 3.3 leads to a frequency variation of 100 MHz at 5.4 GHz, i.e., a reasonable sensitivity. The sensor of [84] is a transmission-mode resonant sensor consisting of a line loaded with an open complementary spit ring resonator (OCSRR). In this sensor, oil adulteration is emulated by introducing a certain percentage of a type of oil in another one, and the output signal is the resonance frequency variation. All these three sensors ([84]-[86]) exploit frequency variation, whereas in the sensors of the present work, phase variation is the considered sensing mechanism. This eases the implementation of the associated electronics in operational environment, where vector network analyzers should be avoided. Note that the reported sensors of this paper only require an electronic oscillator, or a voltage-controlled oscillator (VCO) tuned to the operating frequency. By contrast a sweeping interrogation signal is necessary in the frequency-variation sensors of [84]-[86].

To end this section, let us mention that an alternative approach to enhance sensor resolution and sensitivity that uses active circuitry has been proposed in several works [88]-[90]. Nevertheless, these sensors exploit resonance frequency variation, rather than phase variation, and therefore, a comparison with the sensors of this paper and those in Table I is meaningless. Nevertheless, a qualitative advantage of the sensors of this paper over those presented in [88]-[90] concerns the fact that they are fully passive.

## V. CONCLUSION

In conclusion, the effects of losses on the sensitivity of reflective-mode phase-variation sensors based on a set of cascaded high/low impedance inverters terminated with a distributed (either a quarter- or a half-wavelength) resonator, the sensitive element, have been studied. We have analyzed the sensitivity of the phase of the reflection coefficient, the considered output variable, with the dielectric constant of the MUT, the input variable. The main relevant conclusion of the work concerns the fact that, through a proper sensor design, MUT losses contribute to boost up the sensitivity in the limit of small perturbations. This aspect has been validated by considering the design of three liquid (fluidic) sensors devoted to the measurement of the dielectric constant of oil samples, two of them operating in the so-called low-loss regime, and the other one working under the high-loss regime. It has been shown that in the low-loss regime, with the attenuation factor of the sensing line below a certain threshold that depends on the characteristic impedance of the sensing line and inverters, the sensitivity is negative, whereas it switches to a positive value when the attenuation constant is above that threshold value (high-loss regime). The achieved sensitivities in the limit of small perturbations for the fabricated sensors have been found to be $S_{max}$ = –101.70º (sensor with a single inverter stage operating in the low-loss regime), $S_{max}$ = +206.66º (sensor with two inverters operating in the high-loss regime), and $S_{max}$ = –502.80º (sensor with two inverters operating in the low-loss regime). The high sensitivity in the latter sensor has been instrumental to detect the deterioration of edible oil by usage (particularly by subjecting it to subsequent frying cycles of potatoes).

## APPENDIX A

A variation in the phase of the reflection coefficient, $\phi_\rho$, can be due to a change in both the dielectric constant, $\varepsilon_{\text{LUT}}$, and the loss tangent, $\tan\delta_{\text{LUT}}$ (or attenuation constant, $\alpha$, intimately related with the loss tangent) of the liquid under test (LUT). Thus, a variation in the phase of the reflection coefficient should actually be expressed as

$$\Delta\phi_\rho = \frac{d\phi_\rho}{d\varepsilon_{\text{LUT}}}\,\Delta\varepsilon_{\text{LUT}} + \frac{d\phi_\rho}{d\tan\delta_{\text{LUT}}}\,\Delta\tan\delta_{\text{LUT}} \qquad \text{(A1)}$$

where two sensitivities are included, i.e., the one with $\varepsilon_{\text{LUT}}$, given by (1) and (2), and the one with $\tan\delta_{\text{LUT}}$, namely:

$$\frac{d\phi_\rho}{d\tan\delta_{\text{LUT}}} = \frac{d\phi_\rho}{d(\alpha l_s)}\cdot\frac{d(\alpha l_s)}{d\tan\delta_{\text{LUT}}} \qquad \text{(A2)}$$

where the explicit dependence of $\phi_\rho$ with $\alpha l_s$ is apparent in expressions (9) and (10).

Let us next calculate the derivative $d\phi_\rho/d(\alpha l_s)$ that appears in (A2). Such derivative, for the case of a sensor based merely on the 90º, or 180º, sensing line (i.e., with $N = 0$) is:

$$\begin{aligned}\frac{d\phi_\rho}{d(\alpha l_s)} &= \\ &= \frac{-1}{1+\left(\frac{N}{D_1}\right)^2}\frac{2Z_s\sin 2\phi_s\{Z_0\sinh 2\alpha l_s - Z_s\cosh 2\alpha l_s\}}{D_1^2} + \\ &+ \frac{1}{1+\left(\frac{N}{D_2}\right)^2}\frac{2Z_s\sin 2\phi_s\{Z_0\sinh 2\alpha l_s + Z_s\cosh 2\alpha l_s\}}{D_2^2} \end{aligned} \qquad \text{(A3)}$$

where $N$, $D_1$ and $D_2$ are defined in expressions (12). The derivative (A3) can be rewritten as

$$\begin{aligned}\frac{d\phi_\rho}{d\alpha l_s} &= -\frac{2Z_s\sin 2\phi_s\{Z_0\sinh 2\alpha l_s - Z_s\cosh 2\alpha l_s\}}{D_1^2+N^2} + \\ &+ \frac{2Z_s\sin 2\phi_s\{Z_0\sinh 2\alpha l_s + Z_s\cosh 2\alpha l_s\}}{D_2^2+N^2} \end{aligned} \qquad \text{(A4)}$$

Since the interest in this work is the implementation of very high sensitive sensors, useful to detect tiny variations of the LUT in the vicinity of the reference LUT, it is apparent that the derivative (A4) must be obtained in the limit of small perturbations of $\tan\delta_{\text{LUT}}$ and $\varepsilon_{\text{LUT}}$ with regard to $\tan\delta_{\text{REF}}$ and $\varepsilon_{\text{REF}}$. Therefore, (A4) must be evaluated for either $\phi_s = (2n + 1)\cdot\pi/2$ or $\phi_s = n\pi$ (the electrical lengths of the sensing line corresponding to the REF material). For these specific phases, the derivative (A4) is null, and for this main reason, the second term in the right-hand side of (A1) can be obviated (as it has been done in the sensitivity analysis if section II). This result is also generalizable to a sensor with an arbitrary number of inverter sections, $N$.

## REFERENCES

[1] F. Martín, P. Vélez, J. Muñoz-Enano, L. Su, *Planar Microwave Sensors*, Wiley/IEEE Press, Hoboken, NJ, USA, 2022.
[2] M. Abdolrazzaghi, V. Nayyeri, F. Martín, "Techniques to Improve the Performance of Planar Microwave Sensors: A Review and Recent Developments", *Sensors*, vol. 22, paper 6946, 2022.
[3] D. Girbau, Á. Ramos, A. Lazaro, S. Rima, and R. Villarino, "Passive wireless temperature sensor based on time-coded UWB chipless RFID tags," *IEEE Trans. Microw. Theory Techn.*, vol. 60, no. 11, pp. 3623–3632, Nov. 2012.
[4] W. M. Abdulkawi and A. F. A. Sheta, "Chipless RFID sensors based on multistate coupled line resonators," *Sens. Act. A: Phys.*, vol. 309, paper 112025, Jul. 2020.
[5] J. Yeo, J. I. Lee, and Y. Kwon, "Humidity-sensing chipless RFID tag with enhanced sensitivity using an interdigital capacitor structure," *Sensors*, vol. 21, paper 6550, 2021.
[6] E. M. Amin, M. S. Bhuiyan, N. C. Karmakar, and B. Winther-Jensen, "Development of a low cost printable chipless RFID humidity sensor," *IEEE Sensors J.*, vol. 14, no. 1, pp. 140–149, Jan. 2014.
[7] C. Occhiuzzi, A. Rida, G. Marrocco, and M. Tentzeris, "RFID passive gas sensor integrating carbon nanotubes," *IEEE Trans. Microw. Theory Techn.*, vol. 59, no. 10, pp. 2674–2684, Oct. 2011.
[8] R. A. Potyrailo and C. Surman, "A passive radio-frequency identification (RFID) gas sensor with self-correction against fluctuations of ambient temperature," *Sens. Act. B: Chem.*, vol 185, pp. 587–593, 2013.
[9] A. Ebrahimi, W. Withayachumnankul, S. Al-Sarawi, D. Abbott, "High-sensitivity metamaterial-inspired sensor for microfluidic dielectric characterization," *IEEE Sensors J.*, vol. 14, no. 5, pp. 1345−1351, May 2014.
[10] P. Vélez, K. Grenier, J. Mata-Contreras, D. Dubuc, and F. Martín, "Highly-sensitive microwave sensors based on open complementary split ring resonators (OCSRRs) for dielectric characterization and solute concentration measurements in liquids", *IEEE Access*, vol. 6, pp. 48324-48338, Dec. 2018.
[11] N. Hosseini, M. Baghelani, and M. Daneshmand, "Selective volume fraction sensing using resonant-based microwave sensor and its harmonics," *IEEE Trans. Microw. Theory Techn.*, vol. 68, no. 9, pp. 3958–3968, Sep. 2020.
[12] N. Hosseini and M. Baghelani, "Selective real-time non-contact multi-variable water-alcohol-sugar concentration analysis during fermentation process using microwave split-ring resonator based sensor," *Sens. Act. A: Phys.*, vol. 325, pp, 112695, 2021.
[13] C. G. Juan et al., "Study of $Q_u$-Based Resonant Microwave Sensors and Design of 3-D-Printed Devices Dedicated to Glucose Monitoring," *IEEE Trans. Instrum. Meas.*, vol. 70, Art no. 8005716, 2021.
[14] C. G. Juan, E. Bronchalo, B. Potelon, C. Quendo, V. F. Muñoz, J. M. Ferrández-Vicente, and J. M. Sabater-Navarro. 2023. "On the Selectivity of Planar Microwave Glucose Sensors with Multicomponent Solutions," *Electronics*, vol. 12, no. 1, paper 191, 2023.
[15] P. Vélez, J. Muñoz-Enano, K. Grenier, J. Mata-Contreras, D. Dubuc, F. Martín, "Split ring resonator (SRR) based microwave fluidic sensor for electrolyte concentration measurements", *IEEE Sensors J.*, vol. 19, no. 7, pp. 2562-2569, Apr. 2019.
[16] J. Muñoz-Enano, P. Vélez, M. Gil, E. Jose-Cunilleras, A. Bassols, and F. Martín, "Characterization of Electrolyte Content in Urine Samples through a Differential Microfluidic Sensor Based on Dumbbell-Shaped Defect Ground Structures", *Int. J. Microwaves Wireless Technol.*, vol. 12(9), pp. 817-824, 2020.
[17] R. Narang, S. Mohammadi, M.M. Ashani, *et al.* "Sensitive, Real-time and Non-Intrusive Detection of Concentration and Growth of Pathogenic Bacteria using Microfluidic-Microwave Ring Resonator Biosensor," *Sci. Rep.*, vol. 8, paper 15807, 2018.
[18] M. C. Jain, A.V. Nadaraja, R. Narang, *et al.,* "Rapid and real-time monitoring of bacterial growth against antibiotics in solid growth medium using a contactless planar microwave resonator sensor," *Sci. Rep.*, vol. 11, paper 14775, 2021.
[19] J. Muñoz-Enano, O. Peytral-Rieu, P. Vélez, D. Dubuc, K. Grenier, and F. Martín, "Characterization of the Denaturation of Bovine Serum Albumin (BSA) Protein by Means of a Differential-Mode Microwave Microfluidic Sensor Based on Slot Resonators", *IEEE Sensors J.*, vol. 22, no. 14, pp. 14075-14083, July, 2022.
[20] J. Naqui and F. Martín, "Transmission lines loaded with bisymmetric resonators and their application to angular displacement and velocity

sensors," *IEEE Trans. Microw. Theory Techn*., vol. 61, no. 12, pp. 4700–4713, Dec. 2013.

[21] A. K. Horestani, J. Naqui, D. Abbott, C. Fumeaux, and F. Martín, "Two-dimensional displacement and alignment sensor based on reflection coefficients of open microstrip lines loaded with split ring resonators," *Elec. Lett.*, vol. 50, pp. 620–622, Apr. 2014.

[22] A. Ebrahimi, W. Withayachumnankul, S. F. Al-Sarawi, and D. Abbott, "Metamaterial-inspired rotation sensor with wide dynamic range," *IEEE Sens. J*., vol. 14, no. 8, pp. 2609-2614, Aug. 2014.

[23] J. Mata-Contreras, C. Herrojo, F. Martín, "Application of split ring resonator (SRR) loaded transmission lines to the design of angular displacement and velocity sensors for space applications," *IEEE Trans. Microw. Theory Techn*., vol. 65, pp. 4450–4460, Nov. 2017.

[24] J. Muñoz-Enano, P. Vélez, L. Su, M. Gil, and F. Martín, "A reflective-mode phase-variation displacement sensor", *IEEE Access*, vol. 8, pp. 189565-189575, Oct. 2020.

[25] F. Paredes, C. Herrojo, A. Moya, M. Berenguel-Alonso, D. Gonzalez, J. Bruguera, C. Delgado-Simao, and F. Martín, "Electromagnetic Encoders Screen-Printed on Rubber Belts for Absolute Measurement of Position and Velocity", *Sensors*, vol. 22, paper 2044, 2022.

[26] Z. Mehrjoo, A. Ebrahimi, G. Beziuk, F. Martín, and K. Ghorbani, "Microwave Rotation Sensor Based on Reflection Phase in Transmission Lines Terminated with Lumped Resonators", *IEEE Sensors J*., vol. 23, no. 7, pp. 6571-6580, Apr. 2023.

[27] N. Celik, R. Gagarin, H. -s. Youn and M. F. Iskander, "A Noninvasive Microwave Sensor and Signal Processing Technique for Continuous Monitoring of Vital Signs," *IEEE Ant. Wireless Propag. Lett*., vol. 10, pp. 286-289, 2011.

[28] M. Elgeziry, F. Costa, A. Tognetti and S. Genovesi, "Wearable Textile-Based Sensor Tag for Breath Rate Measurement," *IEEE Sensors J*., vol. 22, no. 23, pp. 22610-22619, Dec. 2022.

[29] M. Puentes, C. Weiß, M. Schüßler, and R. Jakoby, "Sensor array based on split ring resonators for analysis of organic tissues," in *IEEE MTT-S Int. Microw. Symp.*, Baltimore, MD, USA, Jun. 2011, pp. 1−4.

[30] M. Schüßler, C. Mandel, M. Puentes, and R. Jakoby, "Metamaterial inspired microwave sensors," *IEEE Microw. Mag.*, vol. 13, no. 2, pp. 57–68, Mar. 2012.

[31] M. S. Boybay and O. M. Ramahi, "Material characterization using complementary split-ring resonators," *IEEE Trans. Instrum. Meas*., vol. 61, no. 11, pp. 3039−3046, Nov. 2012.

[32] C.-S. Lee and C.-L. Yang, "Complementary split-ring resonators for measuring dielectric constants and loss tangents," *IEEE Microw. Wireless Compon. Lett.*, vol. 24, no. 8, pp. 563−565, Aug. 2014.

[33] C.-L. Yang, C.-S. Lee, K.-W. Chen, and K.-Z. Chen, "Noncontact measurement of complex permittivity and thickness by using planar resonators," *IEEE Trans. Microw. Theory Techn.*, vol. 64, no.1, pp. 247−257, Jan. 2016.

[34] L. Su, J. Mata-Contreras, P. Vélez, F. Martín, "Estimation of the complex permittivity of liquids by means of complementary split ring resonator (CSRR) loaded transmission lines", *2017 IEEE MTT-S International Microwave Workshop Series on Advanced Materials and Processes* (IMWS-AMP 2017), Pavia, Italy, 20-22 Sep. 2017.

[35] L. Su, J. Mata-Contreras, P. Vélez, B. Fernández-Prieto and F. Martín, "Analytical method to estimate the complex permittivity of oil Samples", *Sensors*, 18(4), paper 984, 2018.

[36] B.K, Jha, N, Delmonte, A, Lamecki, M, Mrozowski, M, Bozzi, "Design of microwave-based angular displacement sensor", *IEEE Microw. Wireless Compon. Lett.*, vol. 29 (4), pp. 306-308, Apr. 2019.

[37] M. Saadat-Safa, V. Nayyeri, M. Khanjarian, M. Soleimani and O. M. Ramahi, "A CSRR-Based Sensor for Full Characterization of Magneto-Dielectric Materials," *IEEE Trans. Microw. Theory Techn*., vol. 67, no. 2, pp. 806-814, Feb. 2019.

[38] J. Muñoz-Enano, P. Vélez, M. Gil, F. Martín, "Frequency variation sensors for permittivity measurements based on dumbbell-shaped defect ground structures (DB-DGS): analytical method and sensitivity analysis", *IEEE Sensors J*., vol. 22, no. 10, pp. 9378-9386, May 2022.

[39] J. Naqui, C. Damm, A. Wiens, R. Jakoby, L. Su, J. Mata-Contreras, and F. Martín, "Transmission Lines Loaded with Pairs of Stepped Impedance Resonators: Modeling and Application to Differential Permittivity Measurements", *IEEE Trans. Microw. Theory Techn*., vol. 64, no. 11, pp. 3864-3877, Nov. 2016.

[40] L. Su, J. Mata-Contreras, J. Naqui, and F. Martín, "Splitter/combiner microstrip sections loaded with pairs of complementary split ring resonators (CSRRs): modeling and optimization for differential sensing applications", *IEEE Trans. Microw. Theory Techn*, vol. 64(12), pp. 4362-4370, Dec. 2016

[41] P. Vélez, L. Su, K. Grenier, J. Mata-Contreras, D. Dubuc, and F. Martín, "Microwave microfluidic sensor based on a microstrip splitter/combiner configuration and split ring resonators (SRR) for dielectric characterization of liquids", *IEEE Sensors J*., vol. 17, pp. 6589-6598, Oct. 2017.

[42] A. Ebrahimi, J. Scott, and K. Ghorbani, "Differential sensors using microstrip lines loaded with two split-ring resonators," *IEEE Sens. J*., vol. 18, pp. 5786-5793, 2018.

[43] A. Ebrahimi, G. Beziuk, J. Scott, and K. Ghorbani, "Microwave differential frequency splitting sensor using magnetic-LC resonators," *Sensors*, vol. 20, p. 1066, 2020.

[44] J. Naqui, M. Durán-Sindreu and F. Martín, "Novel sensors based on the symmetry properties of split ring resonators (SRRs)," *Sensors*, vol 11, pp. 7545−7553, 2011.

[45] J. Naqui, M. Durán-Sindreu, and F. Martín, "Alignment and position sensors based on split ring resonators," *Sensors*, vol. 12, pp. 11790−11797, 2012.

[46] A. K. Horestani, C. Fumeaux, S. F. Al-Sarawi, and D. Abbott, "Displacement sensor based on diamond-shaped tapered split ring resonator," *IEEE Sens. J*., vol. 13, pp. 1153–1160, 2013.

[47] A. K. Horestani, D. Abbott, and C. Fumeaux, "Rotation sensor based on horn-shaped split ring resonator," *IEEE Sens. J.*, vol. 13, pp. 3014–3015, 2013.

[48] J. Naqui and F. Martín, "Angular displacement and velocity sensors based on electric-LC (ELC) loaded microstrip lines," *IEEE Sensors J.*, vol. 14, no. 4, pp. 939–940, Apr. 2014.

[49] A. K. Horestani, J. Naqui, D. Abbott, C. Fumeaux, and F. Martín, "Two-dimensional displacement and alignment sensor based on reflection coefficients of open microstrip lines loaded with split ring resonators," *Elec. Lett.*, vol. 50, pp. 620–622, Apr. 2014.

[50] B. Ebrahimi, W. Withayachumnankul, S. F. Al-Sarawi and D. Abbott, "Metamaterial-Inspired Rotation Sensor With Wide Dynamic Range," *IEEE Sensors J*., vol. 14, no. 8, pp. 2609-2614, Aug. 2014.

[51] J. Naqui, J. Coromina, B. Karami-Horestani, C. Fumeaux, and F. Martín, "Angular displacement and velocity sensors based on coplanar waveguides (CPWs) loaded with S-shaped split ring resonator (S-SRR)," *Sensors*, vol. 15, pp. 9628–9650, 2015.

[52] J. Mata-Contreras, C. Herrojo, and F. Martín, "Detecting the rotation direction in contactless angular velocity sensors implemented with rotors loaded with multiple chains of split ring resonators (SRRs)", *IEEE Sensors J*., vol.18, no. 17, pp. 7055-7065, Sep. 2018.

[53] P. Vélez, J. Muñoz-Enano, A. Ebrahimi, C. Herrojo, F. Paredes, J. Scott, K. Ghorbani, and F. Martín, "Single-Frequency Amplitude-Modulation Sensor for Dielectric Characterization of Solids and Microfluidics", *IEEE Sensors J*., vol. 21, no. 10, pp. 12189-12201, May 2021.

[54] C. Damm, M. Schussler, M. Puentes, H. Maune, M. Maasch and R. Jakoby, "Artificial transmission lines for high sensitive microwave sensors," *IEEE Sensors Conf.*, Christchurch, New Zealand, pp.755−758, Oct. 2009.

[55] F.J. Ferrández-Pastor, J.M. García-Chamizo and M. Nieto-Hidalgo, "Electromagnetic differential measuring method: application in microstrip sensors developing", *Sensors*, vol. 17, p. 1650, 2017.

[56] J. Muñoz-Enano, P. Vélez, M. Gil, F. Martín, "An analytical method to implement high sensitivity transmission line differential sensors for dielectric constant measurements", *IEEE Sensors J.*, vol. 20, pp. 178-184, Jan. 2020.

[57] M. Gil, P. Vélez, F. Aznar, J. Muñoz-Enano, and F. Martín, "Differential sensor based on electro-inductive wave (EIW) transmission lines for dielectric constant measurements and defect detection", *IEEE Trans. Ant. Propag*., vol. 68, pp. 1876-1886, Mar. 2020.

[58] J. Muñoz-Enano, P. Vélez, M. Gil, J. Mata-Contreras, and F. Martín, "Differential-mode to common-mode conversion detector based on rat-race couplers: analysis and application to microwave sensors and comparators", *IEEE Trans. Microw. Theory Techn*., vol. 68, pp. 1312-1325, Apr. 2020.

[59] J. Coromina, J. Muñoz-Enano, P. Vélez, A. Ebrahimi, J. Scott, K. Ghorbani, F. Martín, "Capacitively-Loaded Slow-Wave Transmission Lines for Sensitivity Improvement in Phase-Variation Permittivity Sensors", *50th Europ. Microw. Conf*., Utrecht, The Netherlands Sep. 2020.

[60] A. Ebrahimi, J. Coromina, J. Muñoz-Enano, P. Vélez, J. Scott, K. Ghorbani, and F. Martín, "Highly Sensitive Phase-Variation Dielectric

Constant Sensor Based on a Capacitively-Loaded Slow-Wave Transmission Line," *IEEE Trans. Circ. Syst. I: Reg. Papers*, vol. 68, no. 7, pp. 2787-2799, Jul. 2021.
[61] L. Su, J. Muñoz-Enano, P. Vélez, P. Casacuberta, M. Gil, F. Martín, “Phase-Variation Microwave Sensor for Permittivity Measurements Based on a High-Impedance Half-Wavelength Transmission Line,” *IEEE Sensors J*., vol. 21, no. 9, pp. 10647-10656, May 2021.
[62] A. K. Jha, A. Lamecki, M. Mrozowski, and M. Bozzi, “A highly sensitive planar microwave sensor for detecting direction and angle of rotation,” *IEEE Trans. Microw. Theory Techn*., vol. 68, no. 4, pp. 1598–1609, Apr. 2020.
[63] J. Muñoz-Enano, P. Vélez, L. Su, M. Gil, P. Casacuberta, and F. Martín, “On the sensitivity of reflective-mode phase variation sensors based on open-ended stepped-impedance transmission lines: theoretical analysis and experimental validation”, *IEEE Trans. Microw. Theory Techn*. vol. 69, no. 1, pp. 308-324, Jan. 2021.
[64] L. Su, J. Muñoz-Enano, P. Velez, P. Casacuberta, M. Gil and F. Martin, "Highly Sensitive Phase Variation Sensors Based on Step-Impedance Coplanar Waveguide (CPW) Transmission Lines," *IEEE Sensors J*., vol. 21, no. 3, pp. 2864-2872, Feb. 2021.
[65] P. Casacuberta, J. Muñoz-Enano, P. Vélez, L. Su, M. Gil, and F. Martín, "Highly sensitive reflective-mode detectors and dielectric constant sensors based on open-ended stepped-impedance transmission lines", *Sensors*, vol. 20, paper 6236, 2020.
[66] L. Su, J. Muñoz-Enano, P. Vélez, M. Gil, P. Casacuberta, and F. Martín, “Highly sensitive reflective-mode phase-variation permittivity sensor based on a coplanar waveguide (CPW) terminated with an open complementary split ring resonator (OCSRR),” *IEEE Access*, vol. 9, pp. 27928-27944, 2021.
[67] P. Casacuberta, P. Vélez, J. Muñoz-Enano, L. Su, M. Gil, A. Ebrahimi and F. Martín, “Circuit analysis of a Coplanar waveguide (CPW) terminated with a step-impedance resonator (SIR) for highly sensitive one-port permittivity sensing,” *IEEE Access*, vol. 10, pp. 62597-62612, 2022.
[68] A. K. Horestani, Z. Shaterian and F. Martín, "Rotation Sensor Based on the Cross-Polarized Excitation of Split Ring Resonators (SRRs)", *IEEE Sensors J*., vol 20, pp. 9706-9714, Sep. 2020.
[69] P. Casacuberta, P. Vélez, J. Muñoz-Enano, L. Su, and F. Martín "Highly sensitive reflective-mode phase-variation permittivity sensors using coupled line sections", *IEEE Trans. Microw. Theory Techn*., vol. 71, no. 7, pp. 2970-2984, Jul. 2023.
[70] P. Casacuberta, P. Vélez, J. Muñoz-Enano, L. Su, M. Gil-Barba, and F. Martín, "Reflective-Mode Phase-Variation Permittivity Sensors Based on Coupled Resonators", *IEEE Sensors 2022*, Dallas, Texas, USA, Oct. 30 - Nov. 2, 2022.
[71] M. Elgeziry, F. Paredes, P. Vélez, F. Costa, S. Genovesi, F. Martín, "A Method to Retrieve the Output Variables in Reflective-Mode Phase-Variation Sensors", *52nd Europ. Microw. Conf*., Milan, Italy, 20-25 Sep. 2022.
[72] P. Vélez, F. Paredes, P. Casacuberta, M. Elgeziry, L. Su, J. Muñoz-Enano, F. Costa, S. Genovesi, and F. Martín, "Portable Reflective-Mode Phase-Variation Microwave Sensor Based on a Rat-Race Coupler Pair and Gain/Phase Detector for Dielectric Characterization", *IEEE Sensors J*., vol. 23, no. 6, pp. 5745-5756, Mar. 2023.
[73] L. Su, P. Casacuberta, P. Vélez, J. Muñoz-Enano, M. Gil, and F. Martín, "Reflective-Mode Submersible Microwave Sensor", *2022 IEEE Sensors, Dallas, USA*, pp. 1-4.
[74] D.M. Pozar, *Microwave engineering*, 4th Ed., Wiley, Hoboken, USA, 2011.
[75] E. Sikorska, *et al*., “Characterization of edible oils using total luminescence spectroscopy,” *J. Fluorescence*, vol. 14, pp. 25–35, 2004.
[76] J. Yang, K.S. Zhao, Y.J. He, “Quality evaluation of frying oil deterioration by dielectric spectroscopy,” *J. Food Eng*., vol. 180, pp. 69–76, 2016.
[77] S. Pattipaka, A. Joseph, G.P. Bharti, K.J. Raju, A. Khare, D. Pamu, “Thickness dependent microwave dielectric and nonlinear optical properties of Bi0. 5Na0.5TiO3 thin films,” *Appl. Surf. Sci*. vol. 488, pp. 391–403, 2019.
[78] M.E.E. Alahi, A. Nag, S.C. Mukhopadhyay, L. Burkitt, “A temperature compensated graphene sensor for nitrate monitoring in real-time application,” *Sens. Actuators, A*, vol. 269, pp. 79–90, 2018.
[79] O. Chambers, A. Sešek, J.F. Tasicˇ, J. Trontelj, “Fertiliser characterisation using optical and electrical impedance methods,” *Comput. Electron. Agric*., vol. 155, pp. 69–75, 2018.
[80] S. Stevan, L. Paiter, J. Galvão, D. Roque, E. Chaves, “Sensor and methodology for dielectric analysis of vegetal oils submitted to thermal stress,” *Sensors*, vol. 15(10), pp. 26457–26477, 2015.
[81] S. Raadnui, S. Kleesuwan, “Low-cost condition monitoring sensor for used oil analysis,” *Wear*, vol. 259 (7–12), pp. 1502–1506, 2005.
[82] A.Y. Khaled, S.A. Aziz, F.Z. Rokhani, “Capacitive sensor probe to assess frying oil degradation,” *Information Processing in Agriculture*, vol. 2(2), pp. 142–148, 2015.
[83] A. Gongal, S. Amatya, M. Karkee, Q. Zhang, K. Lewis, “Sensors and systems for fruit detection and localization: A review,” *Comput. Electron. Agric*., vol. 116, pp. 8–19, 2015.
[84] P. N. Kakani, C. DS and S. S. Karthikeyan, "Open Complementary Split Ring Resonator Based RF Sensor with Improved Sensitivity for Detection and Estimation of Adulteration in Edible Oils," *2019 TEQIP III Sponsored Int. Conf. Microwave Integrated Circuits, Photonics and Wireless Networks* (IMICPW), 2019, pp. 479-482.
[85] N. K. Tiwari, S. P. Singh and M. J. Akhtar, "Novel Improved Sensitivity Planar Microwave Probe for Adulteration Detection in Edible Oils," *IEEE Microw. Wireless Compon. Lett*., vol. 29, pp. 164-166, Feb. 2019.
[86] M. Erdoğan, *et al*., “Determination of frying sunflower oil usage time for local potato samples by using microwave transmission line based sensors,” *Measurement*, vol. 163, paper 108040, 2020.
[87] M. R. Islam et al., "Tri Circle Split Ring Resonator Shaped Metamaterial With Mathematical Modeling for Oil Concentration Sensing," *IEEE Access*, vol. 9, pp. 161087-161102, 2021.
[88] M. Abdolrazzaghi, N. Kazemi, V. Nayyeri, and F. Martín, “AI-Assisted Ultra-High-Sensitivity/Resolution Active-Coupled CSRR-Based Sensor with Embedded Selectivity”, *Sensors*, vol. 23, pp. 6236, 2023.
[89] N. Kazemi and P. Musilek, "Enhancing Microwave Sensor Performance With Ultrahigh Q Features Using CycleGAN," *IEEE Trans. Microw. Theory Techn*., vol. 70, no. 12, pp. 5369-5382, Dec. 2022.
[90] M. Abdolrazzaghi, N. Katchinskiy, A. Y. Elezzabi, P. E. Light and M. Daneshmand, "Noninvasive Glucose Sensing in Aqueous Solutions Using an Active Split-Ring Resonator," *IEEE Sensors J*., vol. 21, no. 17, pp. 18742-18755, 2021.

**Paris Vélez** (S’10–M’14, SM’21) was born in Barcelona, Spain, in 1982. He received the degree in Telecommunications Engineering, specializing in electronics, the Electronics Engineering degree, and the Ph.D. degree in Electrical Engineering from the Universitat Autònoma de Barcelona, Barcelona, in 2008, 2010, and 2014, respectively. His Ph.D. thesis concerned common mode suppression differential microwave circuits based on metamaterial concepts and semi-lumped resonators. During the Ph.D., he was awarded with a pre-doctoral teaching and research fellowship by the Spanish Government from 2011 to 2014. From 2015-2017, he was involved in subjects related to metamaterial sensors for fluidics detection and characterization at LAAS-CNRS through a TECNIOSpring fellowship cofounded by the Marie Curie program. His current research interests include the miniaturization of passive RF/microwave circuits and the optimization of microwave sensors. Dr. Vélez is a Reviewer for the IEEE Transactions on Microwave Theory and Techniques and for other journals.

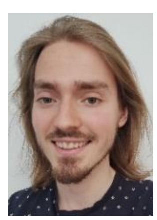

**Xavier Canalias** was born in Sabadell, Barcelona, Spain, in 1999. He received the bachelor's degree in electronic telecommunications engineering and the master’s degree in telecommunications engineering from the Universitat Autònoma de Barcelona (UAB), Spain, in 2021 and 2023, respectively.

**Jonathan Muñoz-Enano** (S’19) was born in Mollet del Vallès (Barcelona), Spain, in 1994. He received the Bachelor's Degree in Electronic Telecommunications Engineering in 2016 and the Master's Degree in Telecommunications Engineering in 2018, both at the Autonomous University of Barcelona (UAB). In July 2022, he obtained the PhD degree within the doctoral programme in Electronics Engineering and Telecommunications in the same university, with the thesis entitled “Highly Sensitive Planar Microwave Sensors for Dielectric

Characterization of Solids, Liquids, and Biosamples." Actually, he is working as a postdoctoral researcher at CIMITEC, Universitat Autònoma de Barcelona. .

**Pau Casacuberta** (GS'22) was born in Sabadell (Barcelona), Spain, in 1997. He received the Bachelor's Degree in Electronic Telecommunications Engineering and Computer Engineering from the Universitat Autònoma de Barcelona (UAB) in 2020, and the master's degree in Telecommunications Engineering in 2022. He received the Collaboration fellowship by the Spanish Government in 2019 for developing his Bachelor's Thesis in highly sensitive microwave sensors based in stepped impedance structures. Furthermore, he is currently working in the elaboration of his PhD, which is focused on the development of microwave sensors for the characterization of the composition of multicomponent liquid substances, with a research grant from FPU Program of the Universities Spanish Ministry.

**Lijuan Su** was born in Qianjiang (Hubei), China in 1983. She received the B.S. degree in communication engineering and the M.S. degree in circuits and systems both from Wuhan University of Technology, Wuhan, China, in 2005 and 2013 respectively, and the Ph.D. degree in electronic engineering from Universitat Autonoma de Barcelona, Barcelona, Spain, in 2017. From Nov. 2017 to Dec. 2019, she worked as a postdoc researcher in Flexible Electronics Research Center, Huazhong University of Science and Technology, Wuhan, China. She is currently a postdoc researcher in CIMITEC, Universitat Autonoma de Barcelona, Spain. Her current research interests focus on the development of novel microwave sensors with improved performance for biosensors, dielectric characterization of solids and liquids, defect detection, industrial processes, etc.

**Ferran Martín** (M'04-SM'08-F'12) was born in Barakaldo (Vizcaya), Spain in 1965. He received the B.S. Degree in Physics from the Universitat Autònoma de Barcelona (UAB) in 1988 and the PhD degree in 1992. From 1994 up to 2006 he was Associate Professor in Electronics at the Departament d'Enginyeria Electrònica (Universitat Autònoma de Barcelona), and since 2007 he is Full Professor of Electronics. In recent years, he has been involved in different research activities including modelling and simulation of electron devices for high frequency applications, millimeter wave and THz generation systems, and the application of electromagnetic bandgaps to microwave and millimeter wave circuits. He is now very active in the field of metamaterials and their application to the miniaturization and optimization of microwave circuits and antennas. Other topics of interest include microwave sensors and RFID systems, with special emphasis on the development of high data capacity chipless-RFID tags. He is the head of the Microwave Engineering, Metamaterials and Antennas Group (GEMMA Group) at UAB, and director of CIMITEC, a research Center on Metamaterials supported by TECNIO (Generalitat de Catalunya). He has organized several international events related to metamaterials and related topics, including Workshops at the IEEE International Microwave Symposium (years 2005 and 2007) and European Microwave Conference (2009, 2015 and 2017), and the Fifth International Congress on Advanced Electromagnetic Materials in Microwaves and Optics (Metamaterials 2011), where he acted as Chair of the Local Organizing Committee. He has acted as Guest Editor for six Special Issues on metamaterials and sensors in five International Journals. He has authored and co-authored over 650 technical conference, letter, journal papers and book chapters, he is co-author of the book on Metamaterials entitled *Metamaterials with Negative Parameters: Theory, Design and Microwave Applications* (John Wiley & Sons Inc.), author of the book *Artificial Transmission Lines for RF and Microwave Applications* (John Wiley & Sons Inc.), co-editor of the book *Balanced Microwave Filters* (Wiley/IEEE Press), co-author of the book *Time-Domain Signature Barcodes for Chipless-RFID and Sensing Applications* (Springer), and co-author of the book *Planar Microwave Sensors* (Wiley/IEEE Press). Ferran Martín has generated 22 PhDs, has filed several patents on metamaterials and related technologies, and has headed dozens of Development Contracts. Prof. Martín is a member of the IEEE Microwave Theory and Techniques Society (IEEE MTT-S). He is reviewer of the IEEE Transactions on Microwave Theory and Techniques and IEEE Microwave and Wireless Components Letters, among many other journals, and he serves as member of the Editorial Board (Associated Editor) of IEEE Transactions on Microwave Theory and Techniques, IET Microwaves, Antennas and Propagation, and Sensors. He is also a member of the Technical Committees of the European Microwave Conference (EuMC) and International Congress on Advanced Electromagnetic Materials in Microwaves and Optics (Metamaterials). Among his distinctions, Ferran Martín has received the 2006 Duran Farell Prize for Technological Research, he holds the *Parc de Recerca UAB – Santander* Technology Transfer Chair, and he has been the recipient of three ICREA ACADEMIA Awards (calls 2008, 2013 and 2018). He is Fellow of the IEEE and Fellow of the IET.